ABSTRACT

Title of Document: MICROFLUIDIC GENERATION OF
                                      ANISOTROPIC CAPSULES.

                                      Xi Lu, Doctor of Philosophy, 2015

Directed by: Professor Srinivasa R. Raghavan
                                      Professor Don L. DeVoe
                                      Depts. of Chemical & Biomolecular Engineering
                                      Depts. of Mechanical Engineering

        Anisotropic particles are those having different properties (physical or chemical) along different directions; in contrast, isotropic particles are identical in all directions. The technical importance of anisotropic structures relies on the fact that a unit with two different characteristics can also exhibit two different functionalities. Such particles have attracted attention due to their potential applications in microrobotics, sensor technologies, drug delivery, and as components in optical devices. In this study, we focus on using microfluidic devices to create anisotropic microcapsules with advanced functionalities. Microfluidic platforms enable the generation of uniform liquid droplets, and we configure these platforms such that the droplets are converted into capsules, i.e., particles with a liquid core and a solid shell. Three different platforms are described, which each generate a unique type of anisotropic capsule.

        In our first study, we describe the microfluidic assembly of Janus-like dimer capsules by the fusion of individual capsules with distinct properties. Microscale aqueous

droplets bearing the biopolymer chitosan are generated *in situ* within a chip and, as they travel downstream, pairs of droplets are made to undergo controlled crosslinking and coalescence (due to a channel expansion) to form stable dimers. These dimers are very much like Janus particles: the size, shape, and functionality of each individual lobe within the dimer can be precisely controlled. To illustrate the diverse functionalities possible, we have prepared dimers wherein one lobe encapsulates paramagnetic nanoparticles. The resulting dimers undergo controlled rotation in an external rotating magnetic field, much like a magnetic stir bar.

In our second study, we describe a new way to create patchy spherical particles. Here, we generate droplets of a chitosan solution containing nanoparticles with an iron (Fe) core and a platinum (Pt) shell. The collected droplets are placed on top of a neodymium magnet to draw the Fe-Pt nanoparticles to their bottom side. The droplets are then crosslinked to convert them into capsules, with the nanoparticles localized on one end as a "patch". The resulting capsules possess both magnetic and catalytic properties. When the capsules are placed in a solution of hydrogen peroxide (H_2O_2), the H_2O_2 is catalytically decomposed by the Pt to generate oxygen bubbles, which cause the capsule to move. Thus, our patchy capsules can act as "micromotors" and their motion can also be controlled by an external magnet.

In our final study, we employ a pulsed-air microfluidic droplet generator to create multi-compartment polymer capsules. These are capsules that have smaller capsules within them. Our technique uses no oil, and is thus very compatible with biological payloads such as proteins or cells. We can also place different payloads within each individual compartment. To demonstrate the unique capabilities of this setup, we have encapsulated different kinds of bacteria in different compartments. Furthermore, we show that the two

bacteria engage in bacterial cross-talk through small molecules known as autoinducers. Specifically, one bacteria produces autoinducer 2 (AI2), which then diffuses across its compartment into the adjacent one, where the second bacteria imbibes the AI2 and in turn, produces a fluorescence response.

MICROFLUIDIC GENERATION OF ANISOTROPIC CAPSULES

By

Xi Lu

Dissertation submitted to the Faculty of the Graduate School of the
University of Maryland, College Park, in partial fulfillment of
the requirements for the degree of
Doctor of Philosophy
2015

Advisory Committee:
Professor Srinivasa Raghavan, Chair
Prof. Don L. DeVoe
Prof. Panagiotis Dimitrakopoulos
Prof. Jeffery B. Klauda
Prof. Zhihong Nie
Prof. Ian M. White

Acknowledgements

First, I would like to thank my advisors, Prof. Srinivasa Raghavan and Prof. Don DeVoe, for providing an opportunity where I was able to be part of their wonderful research groups. Over the course of my graduate study, they have generously provided their time, patience, guidance and support, giving me the flexibility to explore research that was both interesting and challenging. Their philosophies and unique approach in research opened my mind to think like a scientist. Throughout the years, they also taught me invaluable lessons in life, such as kindness, strength and perseverance. They have moved me both professionally and personally, for that I am forever grateful.

Next, I want to give sincere thanks to my committee, Prof. Zhihong Nie, Prof. Panagiotis Dimitrakopoulos, Prof. Jeffrey Klauda, and Prof. Ian White, for their guidance and support. Particularly, Prof. Panagiotis Dimitrakopoulos for his stimulating discussions and the course on Transport Phenomenon, which influenced the direction of my research in droplet microfluidics.

I owe a lot of thanks to my present and past colleagues, in particular Dr. Kunqiang Jiang for generously teaching me everything he knows in the earlier years. In no particular order, I give thanks to Jessica Terrell, Dr. Jikun Liu, Dr. Chenren Shao, Dr. Renee Hood, Omid Rahmanian, Michael Wiederoder, Alex Sposito, Han Choi, Dr. Eric Kendall, Mona Mirzaei, Prakruthi Hareesh, Issac Misri, Dr. Hyunaek Oh, Stephen Banik, Anand Bagal, Dr. Vishal Javvaji, Dr. Bani Cipriano, Charles Kuo, Kunal Pandit, Dr. Chanda Arya, Kevin Diehn, Jasmin Athas, Ankit Gargava, Ankit Goyal, Veena Rao, Brady Zarket, Ian MacIntire, Dr. Matthew Dowling, Salimeh Gharazi, Dr. Joe White, Dr. Will Gibbons. It is

a team effort to complete graduate school and I thank them for their valuable insights and discussions in research. They provided a fun environment where I look forward to coming to work everyday.

To my dear friends. You are the sisters I never had. Thank you for growing with me through this part of my life. You provided the emotional support that I needed throughout the years, and I'm so grateful to have such a tight circle of friends to laugh and cry with.

To Chris, who inspires me to work harder everyday. You put everything in perspective. You have been my loudest cheerleader me during this journey. Thank you for your love and support. I couldn't have done it without you by my side.

To my mom, the person I owe the most to. Thank you for being an amazing mom. To my late grandfather, who was a phenomenal visionary and mentored over 200 students. I remember everything you said when I was younger; I wish I had the opportunity to work with you now.

Table of Contents

LIST OF FIGURES

Chapter 1

Introduction and Overview

1.1. Problem Description and Motivation

Janus, the Roman god of gates and doors, is depicted with two fused heads, each facing in the opposite direction. We use the term Janus to describe one type of anisotropic particles: spheres having two halves (hemispheres), each with a different property.[1] More generally, anisotropic particles are those with different properties (physical or chemical) along different directions. In contrast, isotropic particles have identical properties along all directions. The technical importance of anisotropic structures, such as Janus particles, relies on the fact that a single unit can exhibit two or more different, independent functionalities. For example, one hemisphere of a Janus particle may be designed to be responsive to magnetic fields whereas the other hemisphere may have the ability to target specific biological molecules or species. Such dual or multi-functional capabilities are of much interest for applications. For example, anisotropic particles are already used in applications such as flexible electronic displays (e.g., the technology behind the Amazon Kindle reader),[2] drug delivery,[3-5] sensors,[6,7] and microrobotics.[8-13]

Recently, many methods have been published to make anisotropic or Janus particles using conventional batch synthesis[14-19] or using microfluidic routes.[20-23] Microfluidic platforms are routinely used to generate highly uniform droplets of controlled size (this sub-field is called "droplet microfluidics"). These platforms need to be modified to allow the synthesis of anisotropic particles.[5,6,12,22-28] While several methods have been published,

researchers continue to seek new routes that can either (a) synthesize a particular class of anisotropic particles in a *simpler* manner or at *lower cost*; or (b) synthesize anisotropic particles with a *novel structure or shape* that was not possible by earlier techniques. The search for such new routes is at the heart of the present dissertation.
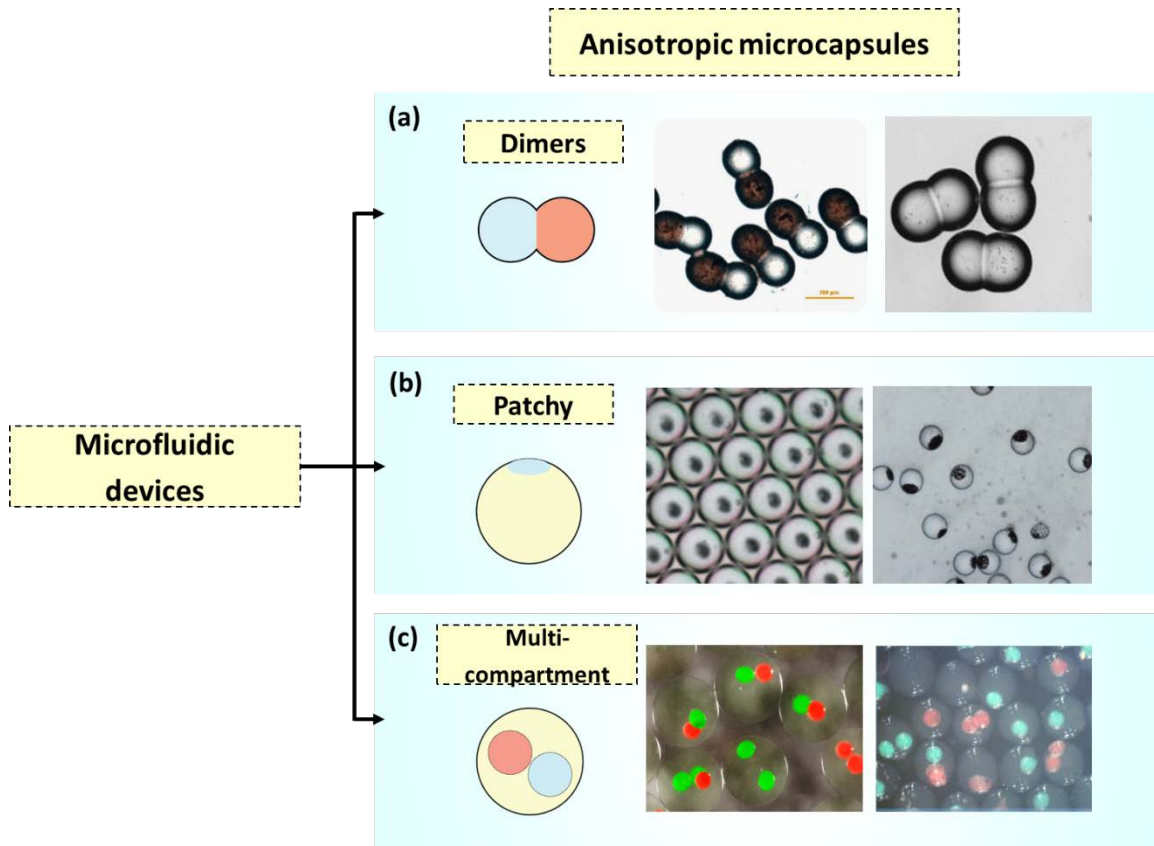
Figure 1.1. The different types of anisotropic microcapsules synthesized in this work. (a) dimer capsules (Chapter 3); (b) patchy capsules (Chapter 4); and (c) multicompartment capsules (Chapter 5). In each case, a different microfluidic platform is used.

1.2. Proposed Approach

In this dissertation, we will describe three routes for synthesizing different types of anisotropic particles (Figure 1.1). We refer to these structures as "capsules", i.e., they have a core that is typically liquid or semi-solid, and a more rigid shell. The three

approaches each use a different type of microfluidic platform (either a chip or capillary tubing). Moreover, these result in three different and unique types of capsules, as shown Figure 1.1, and this is further described below.

1.2.1. Janus-Like Dimer Capsules

Our first study (Chapter 3) is on the microfluidic assembly of Janus-like dimer capsules (Figure 1.1a). Here, we demonstrate the continuous assembly of "dimers" using a microfluidic chip. Soluble precursors are fed into the chip, and two droplets, slightly differing in size are generated. These droplets are then crosslinked on-chip and fused at their interface to form a dimer. The dimers are very much like Janus particles: the size, shape, and functionality of each lobe within the dimer can be precisely controlled. We demonstrate applications for these dimers by incorporating different nanoparticles in each of the dimer lobes. It is notable that all the steps for forming dimers are accomplished continuously on-chip without manual intervention. This aspect mimics the series of unit operations that take place in a chemical factory, and we thus refer to our microfluidic platform as a "microfactory".

1.2.2. Patchy Capsules as Micromotors

In Chapter 4, we present a new class of patchy spherical capsules synthesized off-chip from microfluidically generated droplets (Figure 1.1b). First, nanoparticles with an iron (Fe) core and a platinum (Pt) shell are synthesized in-house using readily available chemicals. These nanoparticles are then encapsulated in a biopolymer solution, and droplets of the mixture are generated using a microfluidic setup. The collected droplets are

placed on top of a neodymium magnet to draw the Fe-Pt nanoparticles to their bottom side. The droplets are then crosslinked to convert them into capsules, with the nanoparticles localized on one end as a "patch". The resulting capsules possess both magnetic properties due to the Fe and catalytic properties due to the Pt. In particular, the capsules can act as micromotors, i.e., they can move in the presence of a chemical fuel (hydrogen peroxide) and they can also be steered by an external magnet.

1.2.3. Multi-Compartment Capsules

In Chapter 5, we employ a pulsed-air microfluidic droplet generator to create multi-compartment polymer capsules (Figure 1.1c). These are capsules that have smaller capsules within them, and the design of these structures is inspired by the structure of a eukaryotic cell. Our technique uses no oil, and is thus very compatible with biological payloads such as proteins or cells. We can also place different payloads within each individual compartment. To demonstrate the unique capabilities of such capsules, we encapsulate two different bacteria in their respective compartments, and we show that the two strains engage in bacterial cross-talk through small molecules known as autoinducers. Specifically, one bacteria produces autoinducer 2 (AI2), which then diffuses across its compartment into the adjacent one, where the second strain imbibes the AI2 and in response turns on a gene that expresses a fluorescent protein.

1.3. Significance of This Work

We believe the significance of this work lies in the use of simple approaches to develop new kinds of anisotropic microcapsules. Our approaches are versatile and can generate capsules with diverse functional properties. Some of the structures we have created, such as the multi-compartment capsules in Chapter 5, have been made for the first time. Numerous applications are likely to emerge for these multi-compartment structures, including their use in investigating cross-kingdom signaling (e.g., bacteria to fungi),[24] and also their application as antibacterial agents that can disrupt bacterial cross-talk. In other cases, such as Chapter 3, our technique itself is noteworthy, such as the idea of continuously generating microstructures on-chip in a microfactory. Also, in Chapter 4, the micromotors that we describe, are biodegradable and soft structures, which are unlike other micromotors that have been reported in the past.

Overall, we anticipate that the new directions we set forth in this field will be further explored by other researchers, and will ultimately lead to practical applications in both existing as well as emerging technologies.

Chapter 2

Background

This dissertation is focused on the microfluidic generation of anisotropic microcapsules. In this chapter we will discuss the basics of droplet microfluidics, current techniques used to create anisotropic capsules, different approaches to creating micromotors, and the basics of quorum sensing, which will be used in Chapter 5 in the context of a particular class of capsules.

2.1. Droplet Microfluidics

Droplets are created in a microfluidic device by bringing two immiscible phases into contact at a geometry such as a T-junction (Figure 2.1a). Two separate syringe pumps control the injection of the dispersed phase at a flow rate Q_d (shown in blue; e.g., aqueous) and the continuous phase, typically at a higher flow rate Q_c (shown in yellow; e.g., oil). At the intersection of the T-junction, droplets of the dispersed phase are formed and these move down the channel. Three key dimensionless groups are of interest for droplet microfluidics: the capillary number $Ca = \mu_c U / \sigma$, the flow rate ratio of the dispersed to continuous phase, and the viscosity ratio of the dispersed to the continuous phase. Here U is the droplet velocity [length/time], σ is the interfacial or surface tension [energy/unit area or force per unit length], Q is the volumetric flow rate [length^3/time], and μ is the fluid viscosity [force/length^3·time]. Because the length scale and flow rates are generally small in microfluidics, the effects of inertia and gravity can be ignored. Thus, other dimensionless

groups, such as the Reynolds number $Re = DU\rho/\mu$, which is a ratio of inertial to viscous forces (D is the channel diameter, ρ is the fluid density), remain low as viscous forces dominate at smaller length scales. For similar reasons, the Weber number (ratio of inertial forces to interfacial tension), and Bond number (ratio of gravity to interfacial tension) are also less significant. The important forces are the viscous and interfacial tension forces and Ca captures their relative contributions. Note that the ratio of surface area to volume is generally large for droplets on the micron scale, which is why surface forces are important. The value of Ca ranges from 10^{-3} to 10^{1} depending on the droplet generation device.[25]
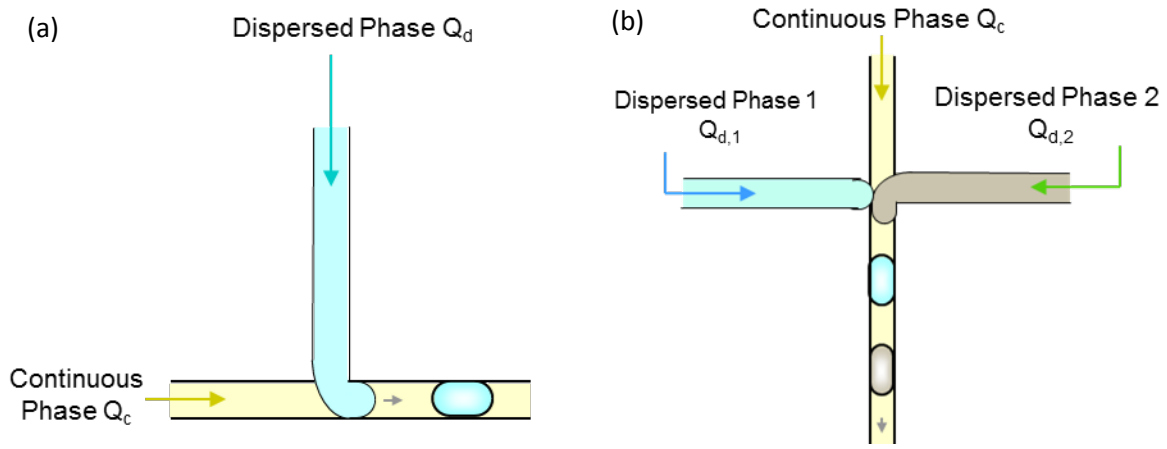
Figure 2.1. Droplet generation at a T-junction (a) and alternating droplet generation in a cross-channel geometry (b).

The flow rate ratio ($FRR = Q_d / Q_c$) of the dispersed to the continuous phase also greatly affects droplet generation. In a regular T-junction depicted in Figure 2.1a, at flow rate ratios below 1, increases in the dispersed phase flow rate Q_d does not affect droplet size.[26] Also, increasing the viscosity of the continuous phase μ_c has no effect on the droplet size. This droplet generation regime corresponds to a low Ca around 10^{-3}, and in this case,

droplet formation is dominated by interfacial tension.[26] Garstecki *et al.* termed this the "squeezing" regime,[26] and explained that the breakup of the droplet depends on the balance of hydrostatic pressure built up when the aqueous droplet fills up the channel. This means that as the emerging droplet blocks the channel, the upstream pressure towards the inlet of the continuous phase increases. The increased pressure leads to a "pinching pressure" which pushes the interface of the two immiscible phases downstream, leading to a thinned "neck" of the aqueous droplet. This "neck" eventually breaks off and a droplet within the continuous phase is formed.[26]

(a)   (b)
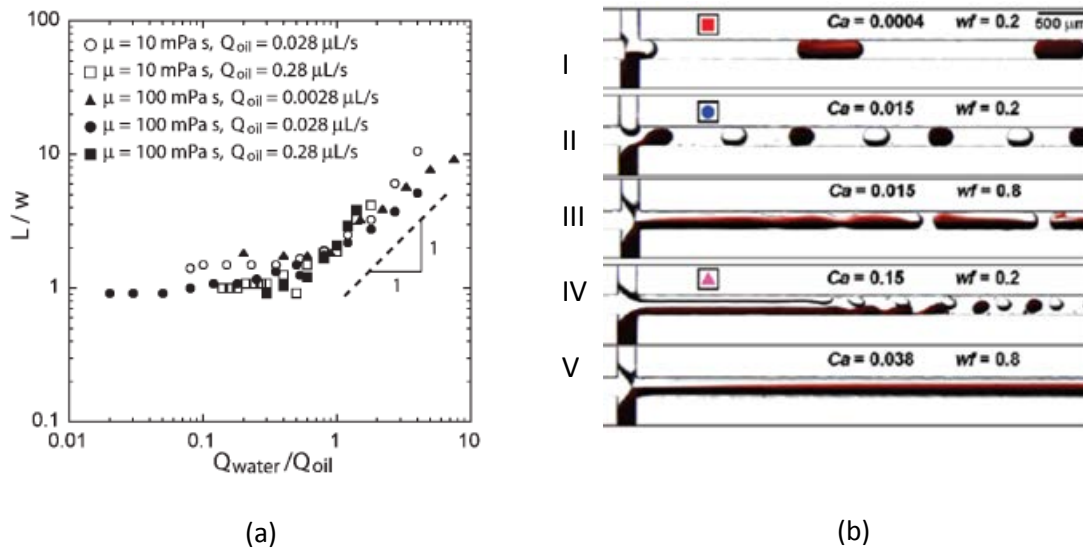
Figure 2.2: (a) Effect of flow rate ratio *FRR* and continuous phase viscosity on droplet size in a T-junction. The x-axis is the $FRR = Q_{water}/Q_{oil}$ = flow rate ratio of the dispersed aqueous phase to the continuous oil phase. L is the length of the droplet in the channel, and w is the width of the channel[26] (b) Effect of capillary number *Ca* and flow rate ratio *FRR* on droplet generation in a cross-channel droplet generator.[27]

The dispersed phase flow rate so far has not been mentioned since the capillary number concerns the continuous phase flow rate Q_c and viscosity μ_c. Once the *FRR* increases above a certain value, increases in the dispersed flow rate Q_d does have a linear

effect on the size of the droplet, as shown in Figure 2.2a. However, even in this regime, changes in continuous phase flow rate Q_c and viscosity μ_c have no effect on droplet size, as seen in Figure 2.2a.

It is possible to modify the T-junction geometry to add an additional inlet, such as in Figure 2.1b, and still maintain two distinct droplet streams. These conditions are satisfied when the *Ca* of the system is around a value of 10^{-2} and the combined dispersed flow rate ($Q_{d1} + Q_{d2}$) is small compared to the continuous phase flow rate Q_c.[27] Droplet formation still occurs in the "squeezing" regime.[27-29] A stable sequence of alternating droplets can thus be generated (Figure 2.2b-II). In contrast, for *Ca* below a critical value, the two dispersed phases meet head on and coalesce (Figure 2.2b-I). At higher *Ca*, the system becomes unstable (Figure 2.2b-IV,V). Also, increasing the combined dispersed phase flow rates causes the two streams to coalesce instead of forming alternate droplets, as seen in Figure 2.2b-III.

2.2. Microfluidic Device Fabrication

In this work, we fabricated microfluidic devices from thermoplastic substrates. Thermoplastic devices can be much more cost-effective than making devices using polydimethylsiloxane (PDMS) via soft lithography. Thermoplastic materials are at least a 100 times cheaper than PDMS. For use at the laboratatory scale, channels on thermoplastic chips with dimensions approaching 50 µm can be directly machined by micro-milling (Figure 2.3, bottom), obviating the need for photolithographic mold production, elastomer casting, and polymer curing. If the same chips have to be mass produced at moderate

volumes, thermoplastics can be rapidly patterned by embossing from a micro-machined mold with cycle times on the order of 10 min (Figure 2.3, top).
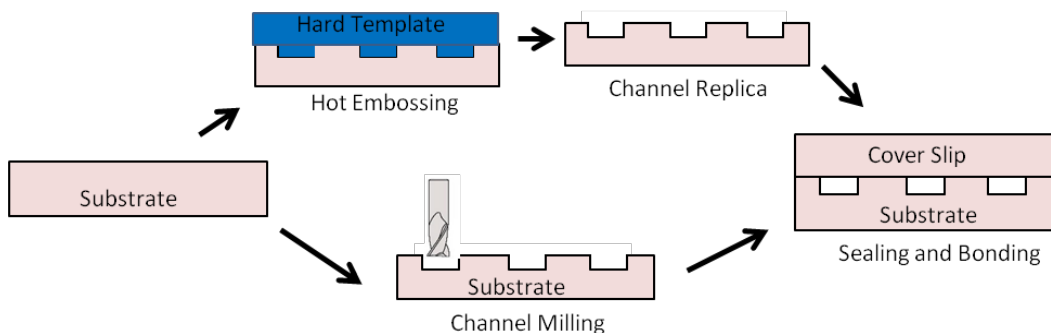
Figure 2.3: Schematic of the fabrication of thermoplastic microfluidic devices. Top route: hot embossing method; bottom route: direct micro-machining.[30]

We also used microfluidic (co-flow) devices assembled from commercially available tubing and glass capillaries, to generate aqueous droplets within an oily continuous phase. By using epoxy resins to seal the open parts, co-flow devices can be made very easily. The schematic for the co-flow device and a photograph of an actual device are shown in Figure 2.4. Here, we insert a glass capillary into Tygon tubing. The Tygon tubing is used for the continuous phase (oil) whereas the dispersed phase (aqueous) is injected into the glass capillary. For water-in-oil droplet formation, the device is used as-is due to the hydrophobic nature of the Tygon tubing. In the case of oil-in-water droplets (not done in this dissertation), a glass capillary must be threaded over the dispersed phase capillary to prevent aggregation of oil droplets at the outer collector.
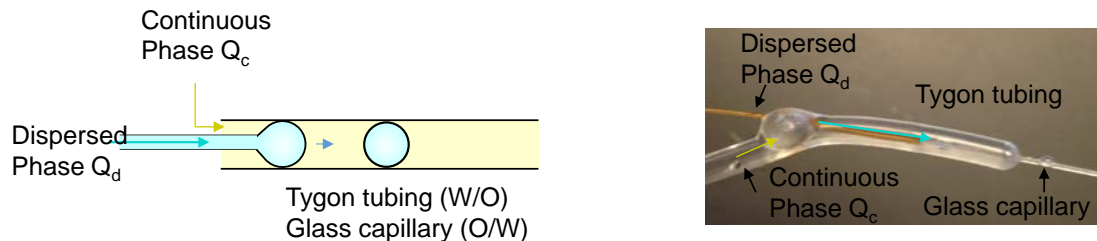
Figure 2.4: Schematic illustration of a co-flow device used for droplet generation (left), and an image of the actual device made with Tygon tubing and glass capillaries.

2.3 Anisotropic Particles and their Microfluidic Synthesis

As mentioned in the Introduction, anisotropic particles are those with different properties (physical or chemical) along different directions. Several microfluidic and lithographic approaches have been used to synthesize such particles.[14,17,19,31] The simplest kind are frequently referred to as Janus particles, i.e., a spherical particle that has two hemispheres of different materials or properties. The term Janus was first coined by Casagrande and used to describe a spherical glass capsule with a hydrophilic hemisphere and a hydrophobic hemisphere.[32] In addition to spheres, Janus particles can also have other shapes, as shown in Figure 2.5a and 2.5b. For example, the barcode particles in Figure 2.5a have a pill-like shape,[6] with one half having a particular sequence of dots, i.e., a bar code. Anisotropy can also be imparted to the interior of a particle, e.g., due to compartmentalization, as shown in Figure 2.5c.[33,34]

We now discuss some of the microfluidic techniques that have been used to make anisotropic (Janus or other) particles. These are classified into three categories in Figure

2.5, including: (a) Flow lithography; (b) Laminar fluidics; and (c) Double and multiphase

flows. Each of these is described in further detail below.
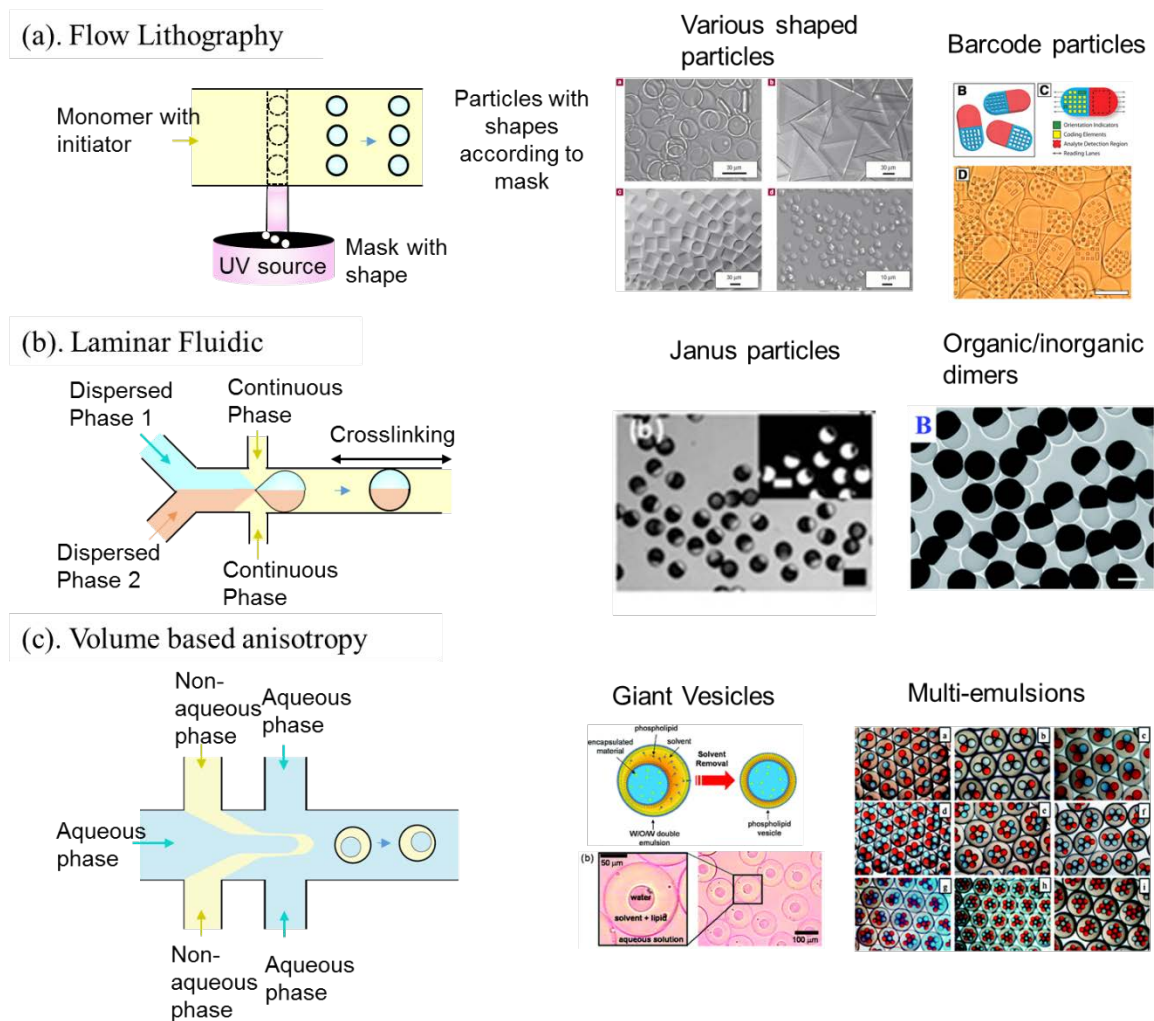
Figure 2.5. Microfluidic techniques for making anisotropic particles. (a) Flow lithography, either continuous[35] or stop flow lithography, which is a process where UV-polymerizable monomers with photoinitiator flow through a device. A mask with the desired particle shape cut out is placed over the UV source on the microscope. Particles are formed through UV crosslinking and collected downstream. (b) Laminar fluidics refers to the laminar flow with minimum mixing between two streams of miscible fluids. This has been exploited to create Janus and tertiary particles and dumbbell shaped particles[20] (c) microfluidics is the only approach where double and multi emulsions can be created with precision.[36] With this approach, oil (o) and water (w) fluids can be combined to create o/w/o or w/o/w droplets with defined internal compartments. Double emulsions have also been used to make polymerosomes[37] and giant vesicles.[33]

Microfluidics coupled with lithography, in cases such as stop-flow and continuous-flow lithography, produces particles that have shapes according to the mask covering the UV lamp (Figure 2.5A).[35] Monomer solutions with initiator are flowed through a PDMS microfluidic device. PDMS is oxygen permeable, which thereby creates a boundary layer at the wall edge resulting in oxidation that prevents UV cross-linking at the bottom wall. This prevents the cross-linked shapes from being immobilized in the channel. Laminar flow behavior can further enhance the functionality of this technique, where different monomer streams that flow in parallel can be crosslinked. Such techniques have been used to create anisotropic "barcode" particles for multiplex protein detection,[6] where one region of the barcode contains antigens for antibody attachment, and the other contains a unique shape based barcode identifier specific to the antigen.

Figure 2.5B shows the typical way to take advantage of the laminar flow behavior in a microfluidic device to make anisotropic particles. Essentially, two or more streams of monomers can be injected in parallel with minimal convective mixing at the interface. The combined stream can then be emulsified into droplets where the different monomers maintain their discrete location even in the droplet. The droplets can then be crosslinked into particles. Microfluidics also makes compartmentalization of internal volumes possible (Figure 2.5C). Double and multiple emulsions are examples of unique morphologies that can be easily achieved by microfluidics, but not in bulk methods. Applications for double emulsions consist of evaporating the middle organic layer to form giant unilamelar vesicles[33] or dewetting the two phases to form polymersomes.[37] One disadvantage with

current methods to form multi-compartment structures is that they all involve two immiscible liquid phases, i.e., oil and water.

2.4. Micromotors
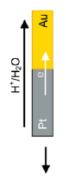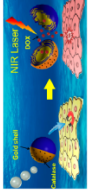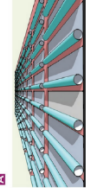
The first example of a micromotor was a PDMS plate with a platinum (Pt) rod inserted on one side; this was shown to undergo autonomous motion (self-propulsion) in a solution of hydrogen peroxide (H_2O_2).[38] This study has spurred a field of research into nano and microscale structures capable of self-propulsion. These structures are termed "microrockets",[5,39] "micromotors",[8,10,11,40-42] "microswimmers",[43] or "microengines".[13] With the variety of names comes an even greater variety of approaches in fabrication. Current designs include bimetallic spheres,[11,44] bimetallic rods,[43,45] tubular structures,[13,39] polymeric capsules,[4,5,46] and other complex shapes.[46,47] All these designs use Pt or another inert metal as a catalyst, while the most common chemical fuel is H_2O_2. When catalyzed by Pt, H_2O_2 decomposes into water and oxygen gas by the reaction in eq 2.1.

$$2H_2O_2 \xrightarrow{\text{Pt}} 2H_2O + O_2 \quad ....(2.1)$$

The oxygen is released in the form of bubbles, which power the motion of the micromotor by an action-reaction mechanism.

Several groups have focused on advancing micromotor technology.[16-19,53-57] The current fuel source, i.e., H_2O_2 is toxic to biological systems. If an alternative fuel source can be found, micromotors could be used for biological applications, such as those envisioned in the movie Fantastic Voyage, where a miniaturized spaceship swims through a patient's veins and delivers medicine to the intended site. Micromotors have been shown to be able to identify a target, pick it up, transport it through a body of liquid, and then drop the target off at a designated location. Micromotors can also isolate circulating tumor cells from biological fluids,[48] cleanup an oil spill from an aqueous solution,[49,50] or move cargo

to form superstructures.[9] Recently, polymeric micromotors have been reported that are also capable of releasing drug in a responsive manner.[4,5]

Type of Micromotors	Schematic	Material	Size (μm)	Methods	Fuel	References
Au-Pt-Ni nanorods		Gold/Pt/Ni	2	Electrochemistry techniques using templates	H_2O_2	Sen and Mallouk, 2005; Sen and Mallouk, 2006
Templated micromotor		Zn/Gold on silica	2	Sputtering of gold on mold, packing silica, electrodeposition	acid	Wang et al., 2014
Polymer based		Gold on PAH/PSS on silica sphere, catalase	8	LBL of polyelectrolyte on silica sphere, then sputter coat gold, cr, HF to dissolve Si	H_2O_2	He et al., 2014
Rolled up microengines		Pt-Fe-Ti microtubes	50	Lithography techniques – ebeam, mask aligner, photoresist	H_2O_2	Mei et al., 2010
Bimetallic spheres		Pt on PS beads	5	E-beam deposition of metal on PS beads	H_2O_2	Schmidt et al., 2011
platinum dimers		Pt on silica sphere	1	Sputter coat pt, cr, then 900C annealing	H_2O_2	Ozin et al., 2010

Figure 2.6: Summary of materials and methods used to create different micromotors. Citations from top: Au-Pt-Ni nanorods;[45,51] templated micromtor;[41] polymer based;[4,5] rolled-up;[9] bimetallic spheres;[44] dimers.[8]

Selecting the method and the material for micromotor synthesis is especially important. A simple synthesis method allows researchers from other disciplines to tackle the problems of finding an alternative fuel or discovering new applications. Current methods require either photolithography or electrochemistry in order to deposit the Pt or other metal on a substrate. A summary of the popular approaches to synthesis is shown in Figure 2.6. Most of these approach require specialized equipment not readily available to traditional chemistry and polymer based facilities. Thus, a flexible, simple, and inexpensive scheme for making micromotors would be beneficial to researchers.

2.5. Biopolymers Used for Making Capsules
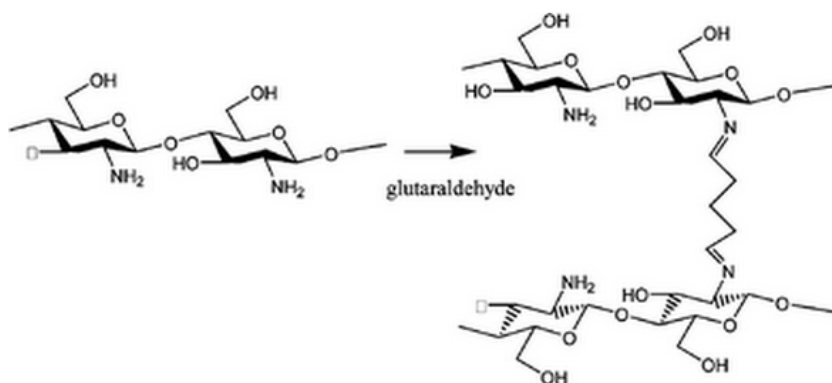
Figure 2.7: Structure of chitosan (left) and a schematic of chitosan being crosslinked by dialdehydes such as glutaraldehyde.[52]

Biopolymers such as alginate and chitosan are frequently explored as vehicles for capsule formation and encapsulation. Chitosan is a polysaccharide with amine groups (structure in Figure 2.7). It is soluble at pH below 5.5, and has a net positive charge due to the protonated free amine group. The free amine group can easily be accessed and

chemically crosslinked with dialdehydes, such as glutaraldehyde (GA) (Figure 2.7).[52] This allows a droplet containing chitosan to be transformed into a capsule or bead when contacted with a solution of GA. Note that GA is soluble in both aqueous as well as nonpolar media. Chitosan can also form capsules through electrostatic interactions with negatively charged surfactants and polymers, such as alginate. Sodium alginate is a linear unbranched polymer made up of blocks of 1,4-linked β-D mannuronic (M) and α-L guluronic (G) residues (Figure 2.8a). It is an anionic biopolymer due to its carboxylate groups. The G-blocks can interact with positively charged multivalent cations (e.g. Ca^{2+}, Sr^{2+}, or Cu^{2+}). Specifically, adjacent linear chains can be cross-linked through formation of "egg-box" junctions with these cations, as shown in Figure 2.8. Thus, a droplet containing sodium alginate can be crosslinked either by contact with positively charged chitosan or by contact with cations like Ca^{2+}.
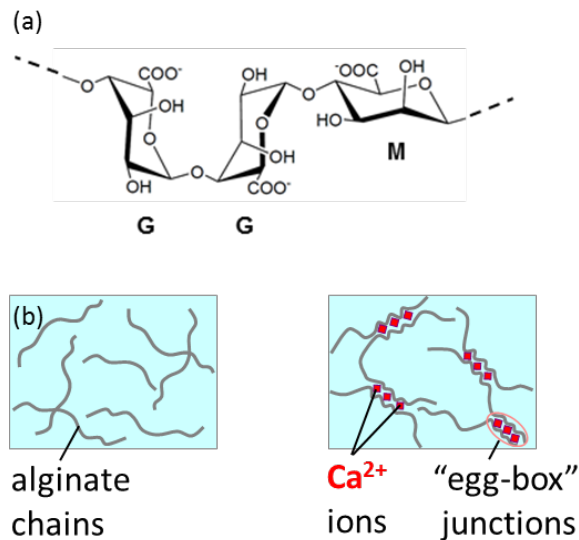
Figure 2.8. (a) structure of alginate with (1-4)-linked β-D-mannuronate (M) and its C-5 epimer α-L-guluronate (G) residues. (b) Schematic demonstrating gelation of alginate upon addition of calcium ions. The zones where crosslinking occurs are called "egg-box" junctions.[53]

18

2.6. Particle Tracking from Images

Particle tracking from time-lapse microscopy images is of key importance for quantitative analysis of dynamic processes. Several software packages exist for tracking of single or multiple particles.[54] In general, a video of the moving particle(s) is converted to a series of stacked images. From the stacked images, the user specifies the first point (p_1) and follows the movement of the particle through a series of images. At the conclusion of the tracking session, a trajectory map is presented of the particular particle in 2-dimensional space. A few nuances of particle tracking are elaborated here.

Time lapse between frames is important in determining speed related parameters. It is important to note the output of the camera in terms of frames per second (fps). Also, when saving files, no compression should be used to distort the metadata. Between point 1 (p_1) and point 2 (p_2), for a 10 fps video, only 0.1 s should have transpired. Video pixels are also important in determining distance travelled, as image data will track in pixels and a conversion will need to be made between pixels and length. It is helpful to keep all settings the same when recording experiments.

For distance calculations, one should note the differences between net distance and net displacement. The former is a scalar where the magnitude of each step is summed up. The latter is a vector based on the initial vs. final position. The instantaneous speed of the particle is given by the segment distance divided by the time lapse between segments.

2.7. Bacterial Quorum Sensing

Quorum sensing is the phenomenon by which unicellular organisms like bacteria coordinate their activities (i.e., act like multicellular organisms) by communicating with each other using small molecules. This can affect bacterial motility, biofilm formation, toxin production and virulence. Many of these multicellular phenotype responses are undesirable to the host environment, especially biofilm formation which is linked to increased antibiotic resistance.[55] Typically, Gram-negative and Gram-positive bacteria communicate via different classes of signaling molecules. However, it was discovered that both types of bacteria also use another molecule called autoinducer-2 (AI-2) for signaling, and hence AI-2 has been dubbed as the universal signaling molecule.[55,56]
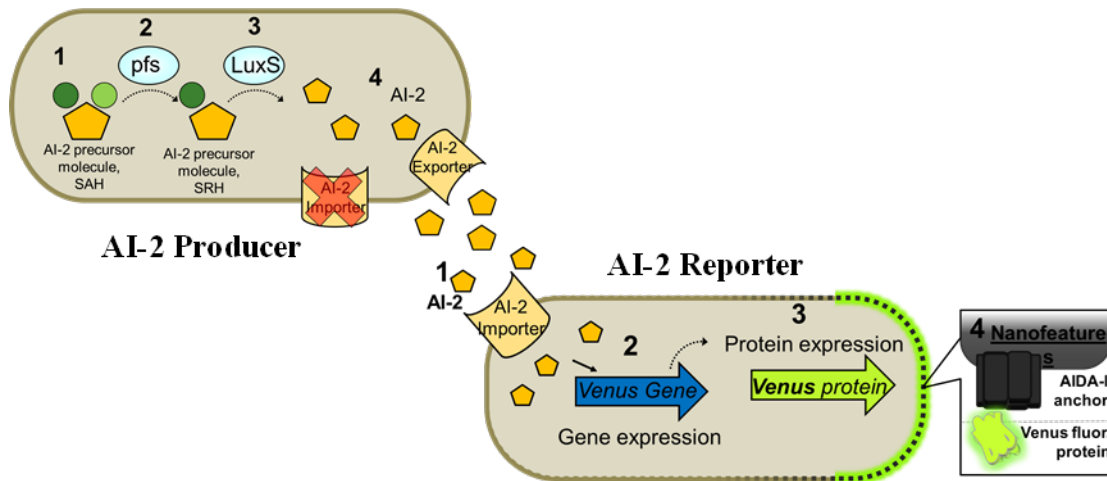
Figure 2.9: Synthesis, secretion, uptake and transduction of AI-2 in E.coli Producer and Reporter strains. In AI-2 Producer: AI-2 precursor SAH is overproduced. Enzymes Pfs and LuxS convert SAH to SRH and DPD, which cyclizes to form AI-2. Also, the Lsr transporter is genetically knocked down. In AI-2 Reporter: AI-2 from the environment is taken up via the Lsr transporter. The imported AI-2 begins a cascade of reactions which include expression of a gene that was inserted into the bacteria, Venus. Venus is a fluorescent protein that is expressed on the surface of the E.coli.

Different groups[57,58] have rewired bacteria's quorum sensing circuits to produce genetically engineered strains that are capable of producing AI-2 or sensing AI-2. For our studies in Chapter 5, we chose a pair of E.coli strains, one of which is capable of producing AI-2 and the other of reporting AI-2 through fluorescence. In the AI-2 producer strain, the AI-2 precursor (S-adenosyl homocysteine) (SAH) is overproduced. Enzymes Pfs and LuxS convert SAH to S-ribosylhomocysteine (SRH) and 4,5-dihydroxy-2,3-pentanedione (DPD), which cyclizes to form AI-2. The AI-2 importer of the producer is removed to avoid self-uptake of the exported AI-2 molecules. In the AI-2 reporter strain, AI-2 from the environment is taken up via the AI-2 importer. The imported AI-2 begins a cascade of reactions which include expression of a gene called Venus that was inserted into the bacteria. Venus is a fluorescent protein that is co-expressed with AIDA-1, which serves as the surface anchor protein; thus, Venus is expressed on the surface of the reporter bacteria.

Chapter 3

Microfluidic Synthesis of Dimer Microcapsules

The results presented in this chapter have been published in the following journal article:

A.X. Lu, KQ. Jiang, D.L. DeVoe and S. R. Raghavan, "Microfluidic Assembly of Janus-Like Dimer Capsules." *Langmuir*, 29 (44), 13624-13629 (2013)

3.1. Introduction

The promise of microfluidic and "lab-on-a-chip" systems is predicated on their ability to miniaturize operations that occur at the macroscale. In particular, a microfluidic chip could be envisioned as a "microfactory"[59] that takes in soluble chemical precursors, builds solid "parts" out of them, and further assembles these parts into a complete object with a specified function. Ideally, such a "microfactory" would operate in a continuous mode without requiring manual intervention. The throughput of completed objects would then be controlled simply by the flow rates of fluids moving through the microfluidic channels. This throughput could then be enhanced by parallel operation of numerous chips. We explored the above concept in a previous study where we used a microfluidic chip to create flexible magnetic chains of microcapsules.[60] However, the process used to make the chains required manual intervention to block and unblock the end of a channel at precise junctures. In the present study, we have developed a scheme that enables continuous synthesis of "dimer capsules", which are two individual biopolymer capsules fused into one stable structure (see Figure 3.1). Our method leverages both the fluid dynamics at the microscale (to induce droplet coalescence within a microchannel) as well as the chemistry of biopolymer crosslinking (to fix the dimer structure).

The dimer structures we create are reminiscent of Janus microcapsules, which have attracted much attention recently.[14,17,20,61] Janus capsules are those having one half with a certain physical or chemical property while the other half has a different property. They derive their name from the Roman god of gates and doors, Janus, who is depicted with two fused heads, each facing in the opposite direction. Most Janus capsules synthesized thus far are spherical in nature and in turn have two distinct hemispherical halves.[17,18] Various microfluidic-assisted synthesis methods have been explored for the synthesis of spherical Janus capsules.[20,21,23,34,36,62-64] For example, the laminar co-flow of two adjacent fluid streams in a microchannel can be broken up into discrete droplets by an immiscible phase, and the resulting droplets can be rapidly photopolymerized in situ to give Janus capsules.[20,62-64] In addition to single capsules with distinct halves, others have also used bulk routes to create dimers of distinct solid colloids[15,19,65] (micro- or nanoparticles) and shown that such dimers can have a Janus-like morphology. The widespread interest in Janus capsules has arisen due to their multifunctional nature:[1] potential applications for these capsules have been demonstrated or envisioned in a variety of areas, including targeted drug delivery[66], emulsion stabilization[67], etc.

Our approach to synthesize Janus-like dimers is quite different from those in previous studies. We use a microfluidic chip to generate aqueous droplets bearing the biopolymer chitosan. Two droplet generators are employed to produce alternating droplets of distinct composition (see Figure 3.1). These droplets are then induced to meet and coalesce downstream by means of an expansion region in the channel. At the same time,

the droplets are also contacted by a continuous flow of glutaraldehyde (GA), which is a known crosslinker for chitosan. The GA converts the droplets into solid capsules and also arrests their coalescence; in effect, the capsules are connected by a neck region to form a stable dimer with each half of the dimer retaining its distinct identity. The entire process of dimer formation is completed within 30 s, with the final structures collected continuously at the channel outlet. Overall our study illustrates how a "microfactory" can be engineered to accomplish a series of steps: droplet formation, fluidic assembly, and chemical linkage, all of which take place on-chip without any manual interruption or manipulation. Two external "handles" are available to tune the morphology of the dimers: the flow rates of each stream, and the channel geometry, specifically the expansion ratio between the expanded and main channels. Stable dimers are obtained only for a subset of these variables, and we will present these results in terms of a "phase diagram" for dimer formation.

3.2. Experimental Section

Materials and Chemicals. Chitosan (medium molecular weight, 190–310K; degree of deacetylation ~ 80%), the nonionic detergent, sorbitan-monooleate (Span 80), hexadecane, and glutaraldehyde solution (grade I, 70% in water), were obtained from Sigma-Aldrich. Magnetic γ-Fe_2O_3 nanoparticles (average surface area ≈ 42 m^2 g^{-1}) were purchased from Alfa Aesar. All chemicals were used as received.

Solution Preparation. 2 wt% chitosan was dissolved in a 0.2 M acetic acid solution, from here on referred to as dispersed phase. For the preparation of magnetic dimers, 0.5 wt% of

γ-Fe2O3 nanoparticles were added into the 2 wt % chitosan solution. The "continuous" phase was prepared by dissolving 2 wt% of Span 80 in hexadecane. Finally, the "incubation" phase was a solution in hexadecane containing 0.2 wt% of Span 80 and 4 wt% of glutaraldehyde. The above mixture was vortexed and sonicated for 30 min before use.

Image Analysis. Bright-light field images were taken by a Nikon Eclipse LV-100 Profilometer Microscope. Capsule sizes (length and radius) were determined using the Nikon Microscope software. Optical monitoring of dimer formation process was performed using an inverted fluorescent microscope (Nikon Eclipse TE2000s).

Chip Fabrication. Microfluidic chips were fabricated from poly(methyl methacrylate) (PMMA) as described previously. PMMA sheets (FF grade; 4" x 4" x 1/16") were purchased from Piedmont Plastics. Microchannels were fabricated by direct mechanical milling onto a PMMA substrate using a 125-µm-diameter end mill (Performance Micro Tool, TR-2-0050-S) on a Roland MDX-650 CNC milling machine with a depth of 90 µm. Holes for the needle interface and access reservoir were drilled into the substrate plate using a 650 µm drill bit and a 2 mm diameter drill bit, respectively. The machined PMMA plate was then sequentially cleaned by deionized (DI) water and isopropyl alcohol, then sonicated for at least 1 h to remove milling debris, followed by a 24 h conservation in a 40 °C vacuum oven to remove the residual solvents. After the vacuum drying, both the processed PMMA and a raw PMMA chip were oxidized by an 8 min exposure to ultraviolet (UV) light in the presence of ozone. The oxidized PMMA wafers were immediately mated together and thermo-bonded at 85°C using a Carver AutoFour hot press under a pressure

of 3.45 MPa for 15 min. The world-to-chip interfaces were established by inserting hypodermic stainless steel needles into the 650 µm diameter mating holes. Precision syringe pumps (PHD 2000, Harvard Apparatus) were used to control the infusion of fluids into the chip.
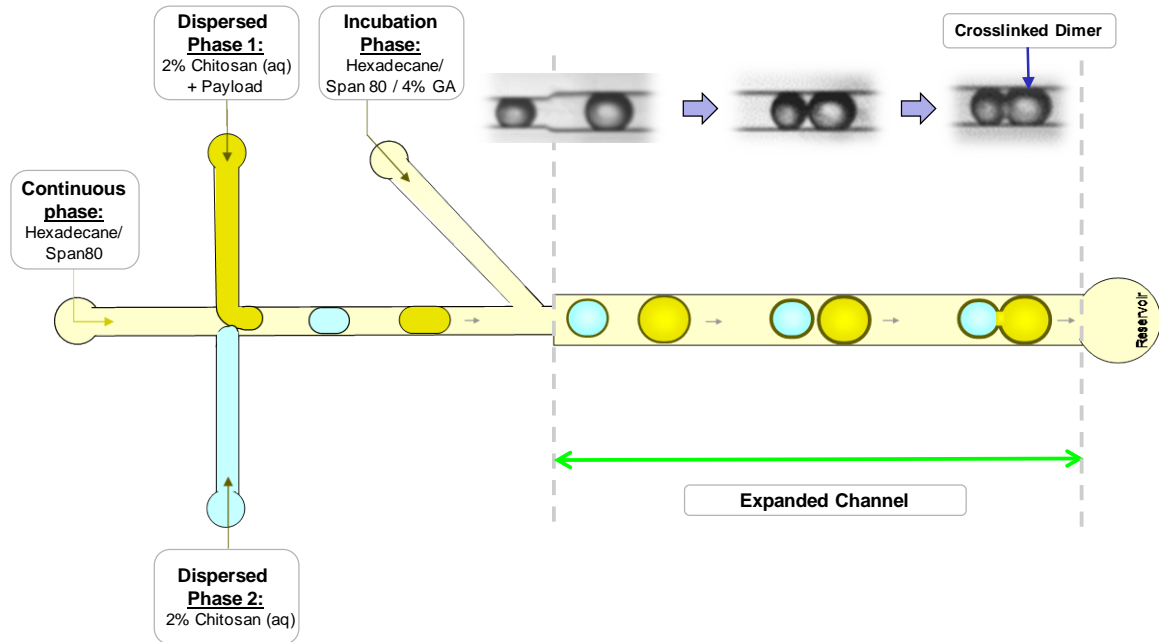
Figure 3.1. Schematic of the microfluidic setup for generating Janus-like dimer capsules. In the cross-channel geometry, two aqueous dispersed phases are contacted by an oily continuous phase. The dispersed phases are aqueous solutions of the biopolymer chitosan (with appropriate payloads). At the T-junction, alternating droplets of the dispersed phases are formed. Dispersed phase 1 flows at a higher flow rate Q_1 and thus generates a larger droplet compared to dispersed phase 2 (flow rate Q_2). As the droplets move down the channel, they are met by a flow of the incubation phase, which contains the crosslinker GA. Subsequently, the droplets enter an expanded channel region, with the expansion inducing the droplets to meet. The droplets are partially crosslinked by GA when they begin to coalesce and the result is that they merge to form a crosslinked dimer. Photographs of the droplets merging into a dimer are shown at the top of the figure. Note that the two lobes of the dimer retain their distinct identity (no mixing of their internal contents) and are connected by a neck region. Ultimately, the dimers are collected in the reservoir at the end of the channel.

Chip design for dimer formation is described in Figure 3.1 and the accompanying text. In addition to the elements shown in Figure 3.1, one optional element was used in some cases to further facilitate droplet formation. This was to introduce a geometric constriction[68] in the shape of a toothcomb structure to the channel at the end of the expanded region and prior to collection in the reservoir. The constriction segment ensured that any capsule pairs that did not merge in the straight channel would merge in this region before leaving the outlet. Note that the toothcomb was not an essential element in the design: dimers could be formed without the toothcomb. However, the constriction is a helpful element for coalescence, as noted by other researchers.[68-70]

3.3. Results and Discussion

The microfluidic chip used in our study has the design shown in Figure 3.1. Droplets are generated by contacting an aqueous dispersed phase and an oily continuous phase at a T-junction. Two dispersed phases are used in a cross geometry to produce alternating droplets with different composition and sizes. Both dispersed phases contain 2 wt% of the aminopolysaccharide, chitosan dissolved in 0.2 M acetic acid. Different materials such as magnetic or metallic nanoparticles or fluorescent dyes can be included in the dispersed phases to provide distinct functional properties to each of the droplets. By controlling the flow rates of the dispersed phases, we can dictate the sizes of the droplets.[27-29] For our purpose, it is essential that the droplets sizes be different, and more specifically, we ensure that within each pair of droplets, the leading droplet is larger than the trailing one. The larger droplet radius is designated as R_1 and the flow rate of its dispersed phase is Q_1; similarly the smaller droplet corresponds to a radius R_2 and a flow rate Q_2.

To convert the chitosan-bearing droplets into stable capsules, a stream of 4 wt% glutaraldehyde (GA) dissolved in oil is introduced downstream. GA is a bifunctional molecule that crosslinks the free amines on chitosan. Given enough contact time, the crosslinking by GA will result in a shell around each droplet. However, in the present case, we induce the droplets to pair up (partially coalesce) before they are fully crosslinked. This is done by introducing an expansion zone in the downstream portion of the channel. As pairs of droplets travel down the expanded channel, they both slow down, but the leading droplet is slowed more than the trailing one. As a result, the droplets (which are semi-crosslinked at this stage) meet and partially coalesce within this zone. Simultaneously, the GA continues to crosslink the chitosan and thereby the overall merged structure is fixed into a doublet or dimer. Note that there is negligible mixing between the two halves (lobes) of the dimer because the individual droplets are rapidly "frozen" (by GA crosslinking) midway through the coalescence event. Thus, dimers can be created with tunable lobes containing distinct functional materials. The dimers are then collected in the reservoir. The total on-chip residence time for the two droplets from their generation to collection as a dimer in the reservoir is approximately 30 s. With typical flow rates (0.15 to 0.35 µL/min for the dispersed phases and 1.5 to 2 µL/min for the continuous phase), we generate on average 1 dimer every 1.4 s. From the reservoir, the dimers are pipetted into a collection vial containing 2 wt% Span 80 and 2 wt% GA, where they are further crosslinked for 30 min. The dimers are then sequentially washed in hexadecane and ethanol, and then redispersed in water, where they remain stable and free of aggregation.

We now discuss the conditions for stable dimer formation. Note that the two droplets initially have elongated plug shapes because their volume is larger than can be accommodated in a sphere that spans the initial width of the channel. However, once the droplets reach the wider expansion zone, they relax into more spherical shapes, which is the one that minimizes surface energy. In the absence of GA crosslinking, the two droplets will meet and then fuse into a larger structure. One factor in stable dimer formation is the concentration of GA because it controls the kinetics of crosslinking. The crosslinking has to be rapid enough to fix the dimer shape before the droplets can fuse. This is why it is necessary to use 4 wt% GA (a relatively high concentration). We originally tested 2 wt% GA, but in this case the GA-induced crosslinking was too slow to prevent partial droplet fusion (see Figure 3.4 below).

Two other key variables are involved in dimer formation and these are: (a) the ratio of the initial droplet sizes (R_1/R_2) measured in the expanded channels and (b) the extent of channel expansion. Note that R_1 corresponds to the larger droplet and so $R_1/R_2 > 1$ in all our experiments. The channel expands from an initial width W_1 to a higher width W_2 and we define a channel expansion parameter as $CEP = (W_2 - W_1)/W_1$. Figure 3.2 is a plot of CEP vs. R_1/R_2 and it shows the conditions that correspond to stable dimer formation (indicated by purple circles, collectively encompassed by the dashed oval) as well as the conditions that do not lead to stable dimers (indicated by red diamonds and blue triangles). Figure 3.2 is thus a "phase diagram" for dimer formation. We consider the three cases below.
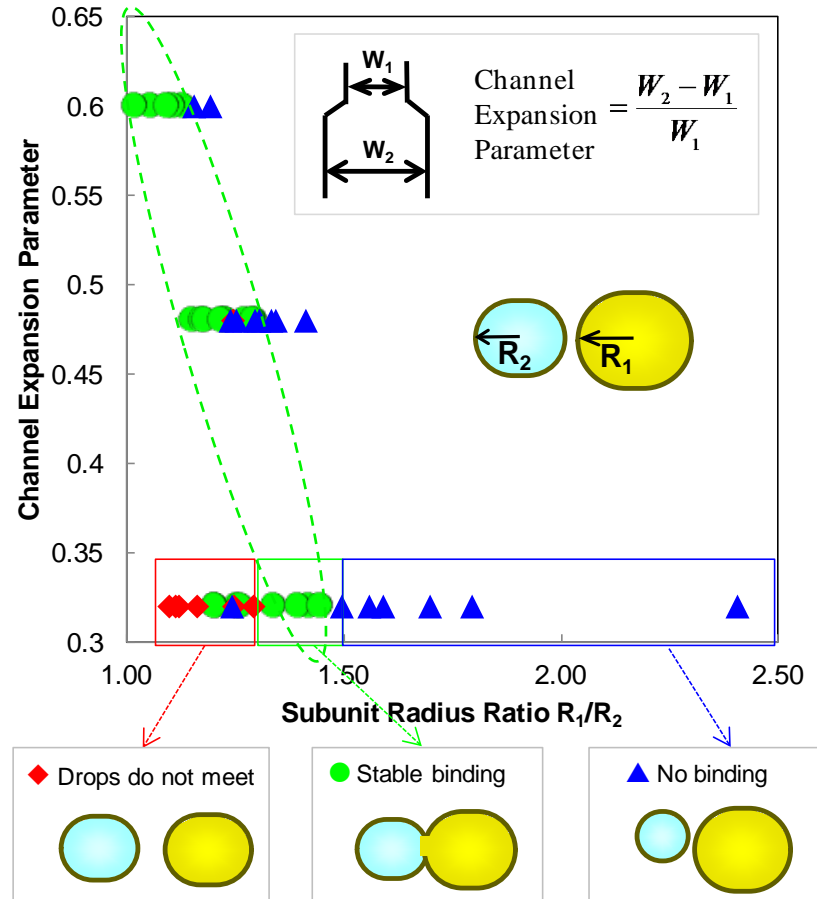
Figure 3.2. "Phase diagram" for dimer formation. This is a plot of the channel expansion parameter (CEP) as a function of the radius ratio R_1/R_2 between the two droplets that form the dimer. The plot shows that stable dimers are formed only for a subset of the conditions studied, which are depicted by green circles. Under these conditions, the droplets meet in the expansion channel and bind to form stable dimers. In contrast, for the conditions marked by red diamonds (typically at low R_1/R_2), the droplets are too similar in size and do not meet in the expansion channel. On the other hand, for the conditions marked by blue triangles (typically at high R_1/R_2), the droplets meet in the expansion channel but do not bind.

First, the red diamonds in Figure 3.2 correspond to the case where R_1/R_2 is not much greater than 1 and the *CEP* is low. In this case, successive droplets simply do not meet in the expansion zone and therefore no dimer is formed. To understand this, we elaborate on the reason why channel expansion forces the droplets to meet. Before entering the

expansion zone, the plug-like droplets fill up the entire channel and both droplets travel at the same velocity (if there was no expansion, the droplets would never meet). As the droplets move from the normal to the expanded channel, they slow down by the law of continuity. Moreover, in the expansion zone, the inset in Figure 3.1 shows that the larger leading droplet (radius R_1) spans the channel whereas the trailing droplet (radius R_2) travels along the center line but occupies only a portion of the channel. From Poiseuille flow for laminar flow[71] between parallel planes, it is known that the fluid velocity assumes a parabolic profile, with a maximum v_{max} at the center line, and zero velocity (no-slip condition) at the channel walls. The mean velocity for this flow profile is 2/3 v_{max}. Thus, a droplet that spans the channel will have a velocity $\approx$ 2/3 v_{max}, whereas a very small droplet that is close to the center line will have a higher velocity that is $\approx v_{max}$. More generally, the smaller trailing droplet will have a higher velocity than the larger one ahead of it, and this allows the two to catch up. However, if R_1 and R_2 are very close, the velocity difference is not enough to ensure that the droplets will be able to catch up within the length of the expanded channel. This explains why no dimers are formed for the conditions marked by the yellow diamonds.

Next, we consider the conditions marked by the blue triangles in Figure 3.2, which correspond to high R_1/R_2 at each *CEP*. In these cases, the leading droplet (R_1) is much larger than the trailing one (R_2). We observe that the droplets meet in the expansion zone, but do not merge. The reasons for this are not clear. One possible factor is that the smaller droplet experiences hydrodynamic lift forces due to inertia, which introduce a component to the droplet velocity that is perpendicular to the primary streamlines. If so, this droplet

will meet its counterpart at an angle and not along the center line of the channel. These conditions may not be conducive to merging of droplets. (An equivalent viewpoint is to assume that the lift forces serve to undo the droplet-droplet bonds.) All in all, we observe stable dimers for moderate values of R_1/R_2 (not too low or high) at each CEP and these conditions are marked by the purple circles. As shown by the inset in Figure 3.1, a stable dimer typically has a neck region between the two adjacent lobes.

Other factors to consider in dimer formation are the lengths of the microfluidic channel segments. In our design (Figure 3.1), the expansion channel is placed close to the GA inlet stream. This is done to ensure that the droplets do not get substantially crosslinked by GA before they meet. That is, dimerization can only occur for droplets that have not been fully converted into capsules. In addition, the expansion channel must be of sufficient length to provide enough time for the dimer to fully form. After the droplets first meet, the film between the droplets has to drain completely for the droplets to merge and crosslink into a dimer. For this, our experiments show that the droplet pair has to remain in contact for about 13 s in the expansion channel before merging is completed. Note that this time is rather large compared to the time required for film drainage in previous droplet coalescence studies, which have been reported to be on the order of 10^{-2} s.[72-74] Evidently, the present case is more complex as it involves a combination of droplet merging as well as chemical crosslinking of each droplet and also of the neck region between the droplets. The crosslinking reaction reduces the mobility of the fluid between the two droplets and thus the film drainage rate,[28,29] which is why the merging process takes a longer time.
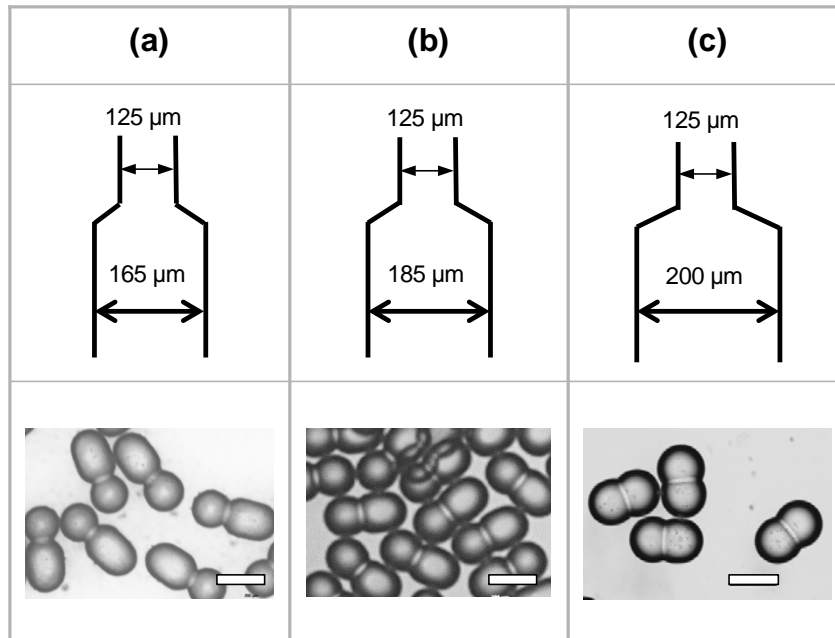
Figure 3.3. Dimers of different morphologies by adjusting the channel geometry and dispersed flow rates. Three different sizes of the expansion channel: (a) 165 µm, (b) 185 µm, and (c) 200 µm were tested, with the main channel maintained at 125 µm. In (a) the dimers assume a "bowling-pin" morphology, with one lobe elongated and the other spherical. In (c) the dimers take on a "snowman" morphology with two nearly-spherical lobes. In (b) the morphology is intermediate between the other two. Scale bar represents 200 µm.

Figure 3.3 shows the morphology of dimers corresponding to different sizes of the expansion channel (with the main channel maintained at 125 µm). For an expansion channel size of 165 µm (the smallest tested), we found that among each pair of droplets, the larger leading one remains plug-shaped in the expansion channel while the smaller trailing one relaxes to a spherical shape. Dimers formed from such pairs of droplets have an elongated shape reminiscent of a "bowling pin" (Figure 3.3a). Note that the bowling pins have a short spherical lobe attached to a longer plug-shaped lobe. If the expansion channel is made wider (185 or 200 µm), then both the leading and trailing droplets relax to spherical shapes in the expansion channel. The resulting dimers have a rounder

morphology and the shape in Figure 3.3c is reminiscent of a "snowman". In this case, the two lobes of the dimers have nearly equal lengths.

(a)   **(b)**

| Incubation Phase: 4% GA | Incubation Phase: 2% GA |
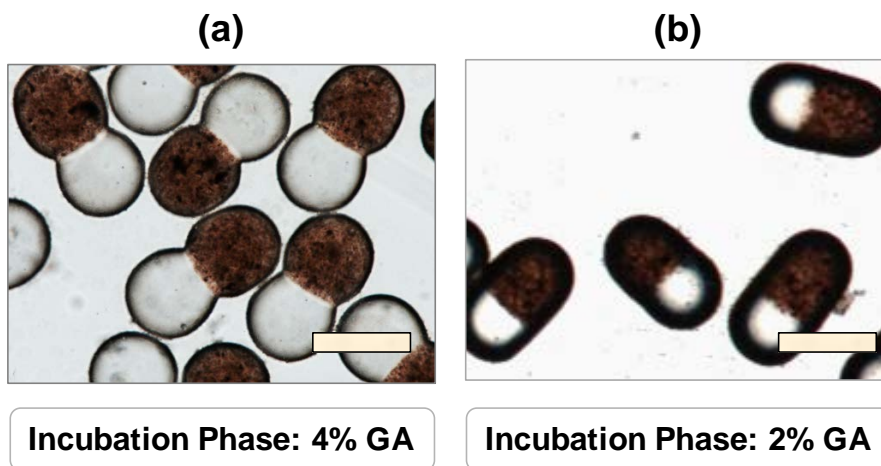
Figure 3.4. Magnetic dimers with MNPs in one lobe. The lobe with MNPs shows a dark color relative to the other lobe. These Janus-like dimers were created by using two dispersed phaes, one of chitosan+MNPs and the other of chitosan alone. The dimers in (a) were formed with 4% GA as the incubation phase: in this case, the contents of the lobes are well-separated. On the other hand, the dimers in (b) were formed with 2% GA as the incubation phase. At this lower concentration of the GA crosslinker, the contents of the two lobes undergo partial mixing and there is no neck region separating the lobes. Scale bar represents 200 μm.

In addition to creating dimers of various morphologies, we are interested in engineering the functional properties of these dimers. As an initial demonstration, we incorporate magnetic nanoparticles (MNPs) into one lobe of our dimer to create Janus-like dimers with an overall magnetic moment. Specifically, we combined 0.5 wt% of the MNPs with the 2 wt% chitosan solution and used this mixture as the dispersed phase for one inlet, whereas the other inlet was just the 2 wt% chitosan solution. Optical micrographs of the resulting snowman-shaped magnetic dimers are shown in Figure 3.4a. The MNP-bearing lobe has a dark brown color whereas the other lobe is colorless. Note the clear separation between the two lobes, which shows that the inner contents of the two lobes do not mix

during dimer formation. Such dimers were produced using 4 wt% GA as the crosslinker. If the GA concentration was reduced to 2 wt%, we obtained the dimers shown in Figure 3.4b. As noted earlier, at this lower GA, crosslinking is not rapid enough to prevent the droplets from partial fusion. Thus, the MNP-bearing droplet and the bare droplet partially fuse, as seen from the dark brown color pervading through most of the pill-shaped dimers in Figure 3.4b. Also, these dimers have no intervening "neck" region between their respective lobes.

The magnetic response of the anisotropic (Janus-like) dimers in Figure 3.4a was tested by placing a Petri dish containing the dimers in water on a standard magnetic stir plate. The rotating magnetic field produced by the stir plate caused the dimers to rotate, much like a microscale magnetic stir bar. This occurs because the dimer acquires a magnetic moment due to the MNPs being localized in one lobe. Note also that the axis of rotation is located within the MNP-bearing lobe, i.e., it is eccentric with respect to the whole particle. The rotation of the dimer induces significant convective mixing in the surrounding fluid close to the dimer. This suggests the possibility of using magnetic dimers for the micro-mixing of fluids within microscale and lab-on-a-chip devices.
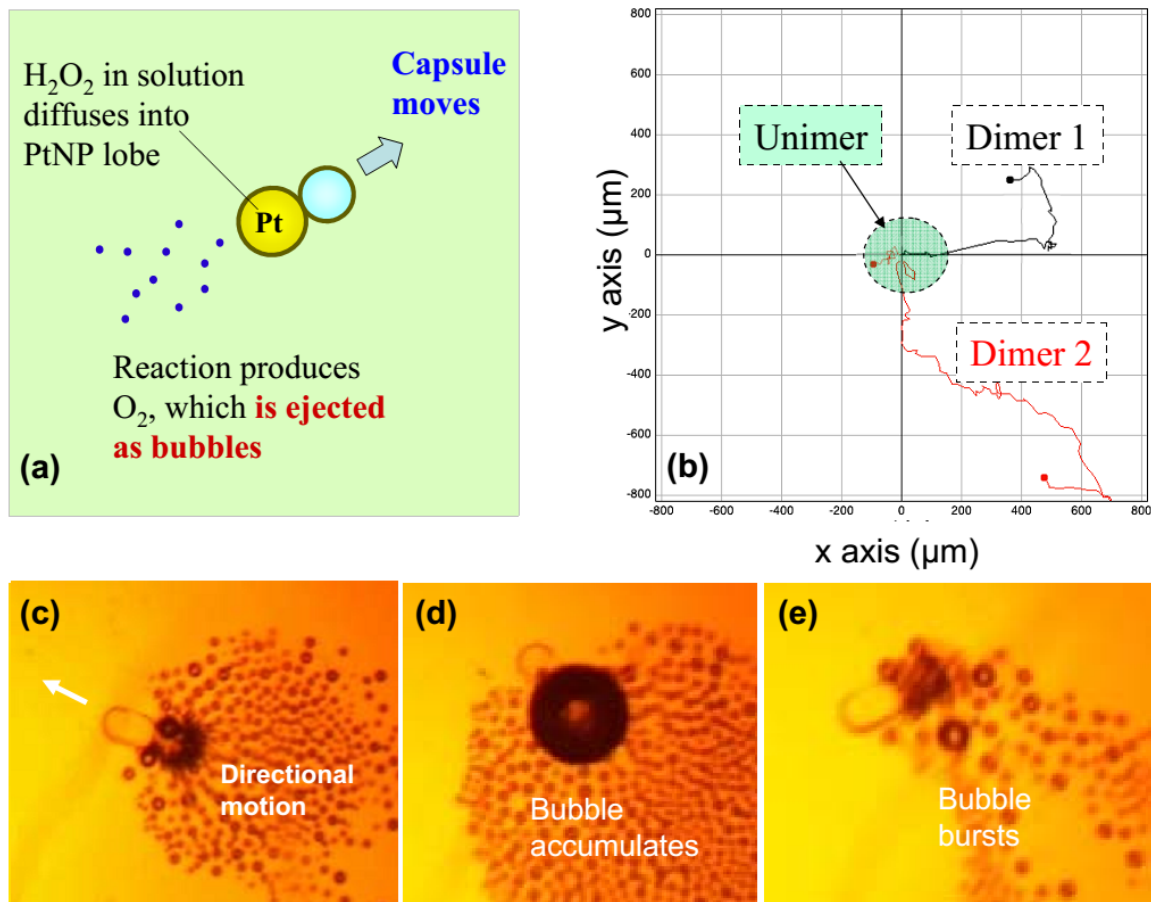
Figure 3.5. Dimer capsules as micromotors. These have PtNPs in one lobe. (a) Schematic depicting the mechanism for self-propulsion in a solution of H_2O_2. (b) 2-D plot of capsule trajectories for three cases. The unimer with PtNPs shows negligible net displacement, whereas the dimers move significantly. (c), (d), (e) Images of dimer capsules moving in H_2O_2 solution. Note that the direction of motion is opposite to that of bubble ejection. In (d), a large bubble accumulates on the surface of the dimer, and in (e), this bubble bursts, which propels the capsule at 20 times its average speed.

In a second application of the dimers, we loaded one lobe of the dimer with platinum nanoparticles (PtNPs), which were synthesized using the Turkevich method. Platinum is known to catalyze the decomposition of hydrogen peroxide (H_2O_2) into oxygen (see eq 2.1 in Section 2.4). The oyxgen bubbles can cause autonomous motion (self-propulsion) of microstructures. To test this possibility, we placed our dimers (with one lobe

containing PtNPs) in a solution of H_2O_2. As shown by the images in Figure 3.5, the dimer undergoes self-propelled motion. The schematic in Figure 3.5a describes the mechanism: the H_2O_2 diffuses into the PtNP-lobe, where the reaction occurs. The O_2 is ejected out of this lobe in the form of bubbles. The dimer then moves in the opposite direction, showing that this is an action-reaction mechanism.

Figure 3.5b compares the trajectories for two cases on a 2-D plot: (a) 2 anisotropic dimer capsules with PtNPs in one lobe; and (b) an isotropic monomer capsule with PtNPs. The net distance travelled by the latter is negligible; instead, this capsule mostly rotates about its own axis. This shows that the anisotropy due to the dimer structure is essential for directionality and motion. From the trajectory, the average speed for the 2 dimer capsules in Figure 3.5b is 150 µm/s over about 50 s of observation time. However, there are periods where a large bubble attaches to the surface of the dimer; this then accumulates further oxygen and grow to a size as large as the dimer itself (Figure 3.5d). Ultimately, this bubble bursts (Figure 3.5e), causing a sudden increase in the speed of propulsion to 2400 µm/s, which is almost 20 times the average speed.

3.4. Conclusions

We have demonstrated the continuous micromanufacturing of Janus-like dimer capsules on a microfluidic chip. Our method involves generating alternating droplets of distinct composition (both based on the biopolymer chitosan) and inducing these droplets to meet downstream by means of an expansion region in the channel. At the same time, a flow of crosslinker (GA) converts the droplet pair into a stable dimer while

also arresting their coalescence. The overall process starting from soluble precursors and culminating in stable dimers takes about 30 s and occurs continuously on-chip without external manual control. Each lobe of the dimer retains its distinct identity giving the overall structure a Janus-like architecture. As an initial example, we create dimers that have a net magnetic moment by including MNPs in one lobe: these structures undergo rotation when placed on a magnetic stir plate. In a second example, we encapsulated PtNPs in one lobe. The PtNPs react with hydrogen peroxide to form oxygen bubbles which can propel the dimer in a directional trajectory. We refer to these as self-propelled micromotors.

Our approach demonstrates that dimer structures can be achieved in a microfluidic device without templates and also without resorting to photo-polymerization. The ability to easily incorporate different functional nanoparticles into each lobe of the dimer is an attractive feature of our approach. Overall, the dimers produced in this study could be explored for many applications such as drug delivery, microrobotics, micromixers and sensors.

Chapter 4

Patchy Capsules as Micromotors

4.1. Introduction

Imagine a capsule that can maneuver through a body of contaminated liquid,[4,5] pick out targets of interest and transport them to a different destination,[44,75] followed by clean-up of contaminants in the liquid.[49] These are all envisioned applications for capsules that are capable of self-propelled motion. These self-propelled capsules, or micromotors, use only the chemical fuel in the environment to drive motion. Ideally, such a system will move without external manipulation, and will continue as long as there is fuel in the surroundings. The speed of the micromotor would then be controlled by changes in fuel concentration. The trajectory or the direction can be guided by an external force, usually by a magnetic field.[9,10,76] Various types of micromotors have emerged in the past decade; however, these are typically synthesized through complex lithographic or electrochemical methods. Moreover, typical micromotors are hard, non-degradable structures. Recently, some researchers have attempted to design micromotors using soft materials such as synthetic polymers.[4,5,46] Here, we report a micromotor that is built using a biocompatible polysaccharide, which makes it a soft and biodegradable structure. This micromotor is capable of all the functionalities of earlier micromotors, such as bubble propulsion, magnetically guided movement, and cargo pick-up and drop-off.

The micromotors we create are spherical capsules with a "patch" of nanoparticles encapsulated at one end of the capsule (see Figure 4.2). The nanoparticles we use have an

iron-oxide core and a platinum (Pt) shell (termed FePt NPs) and are synthesized using the procedure outlined by Mori et al.[77] A solution of the biopolymer, chitosan is combined with the NPs and this serves as the disperse phase in a co-flow microfluidic tubing device (Figure 2.4), with the disperse phase being an oil (hexadecane). The output of the device is an emulsion containing chitosan-FePt NP droplets emulsified in hexadecane. We exploit the magnetic character of the capsules (due to the iron-oxide core) to make patchy capsules. Specifically, the emulsion is placed on top of a neodymium magnet. The magnetic field draws the FePt NPs to the bottom of each droplet. We then use glutaraldehyde (GA), a known crosslinker for chitosan, to convert the droplets into capsules. Our approach is robust and simple; the resulting micromotors are capable of self-propulsion and also have magnetic properties. For self-propulsion, the micromotors are placed in a solution hydrogen peroxide (H_2O_2) (Figure 4.1). The Pt portion of the NPs catalyzes the decomposition of H_2O_2 (see eq 2.1), generating oxygen gas in the form of bubbles. The bubbles are ejected from the patchy capsules, and in turn, the capsules move in the opposite direction (Figure 4.1).
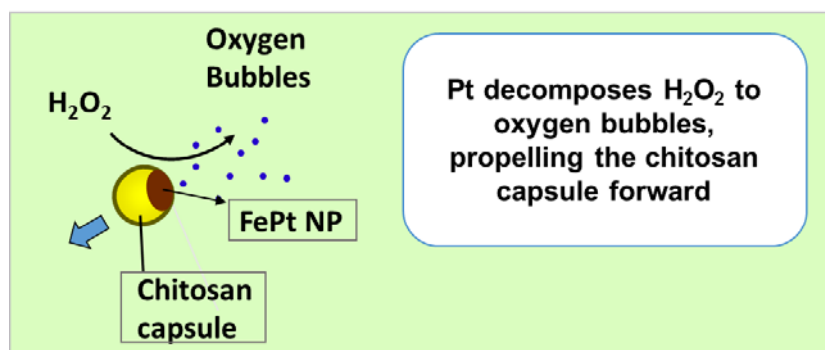
Figure 4.1. Self-propulsion of a chitosan capsule bearing a patch of FePt NPs. The Pt in the NPs catalyses the conversion of H_2O_2 into oxygen. The oxygen gas is ejected as bubbles, thereby propelling the capsule in the opposite direction.

4.2. Experimental Section

Materials and Chemicals. Chitosan (medium molecular weight, 190–310K; degree of deacetylation ~ 80%), the nonionic detergent, sorbitan-monooleate (Span 80), hexadecane, glutaraldehyde solution (grade I, 70% in water), dibenzyl ether, iron pentacarbonyl, platinum(II) acetylacetonate, and oleylamine were obtained from Sigma-Aldrich. Oleic acid was purchased from Alfa Aesar. All chemicals were used as received without further purification.

FePt Nanoparticle Preparation. Particles were made **as** described below.[77] 1.0 mmol of iron pentacarbonyl was mixed with 100 mL of dibenzyl ether in a 500 mL 3 neck flask. The solution was then degassed for 1 hour before heating to 260°C under a nitrogen blanket with vigorous stirring for 10 minutes. 1.0 mmol of oleic acid, 1.0 mmol of oleylamine, and 0.5 mmol of platinum acetylacetonate was dissolved in 2 mL of dibenzyl either and then injected into the flask. The solution was then heated under reflux at 245°C for 1 hour and then left to cool to room temperature. Once cooled, the FePt NPs were centrifuged and washed with toluene and hexane, and the resulting NP were stored in hexane solution. Nanoparticle sizes were measured by dynamic light scattering on a Photocor-FC instrument.

Solution Preparation. 2 wt% chitosan was dissolved in a 0.2 M acetic acid solution. For the preparation of capsules: approximately 10 mL of FePt/hexane solution was vacuum dried overnight which yielded 0.003 g of dry FePt NPs. 5 g of 2 wt% chitosan was directly added to the dry FePt NP, vortexed and sonicated for 30 min before use. The continuous phase was prepared by dissolving 2 wt% of Span 80 in hexadecane. Finally, the incubation

phase was a solution in hexadecane containing 2 wt% of Span 80 and 2 wt% of glutaraldehyde. This mixture was vortexed and sonicated for 30 min before use.

Microfluidic Tubing Device Fabrication. 0.05 cm inner diameter (I.D.) x 0.08 cm outer diameter (O.D.) round glass capillaries (Fiber Optics Center, Inc) was inserted into 100 µm I.D. x 360 µm O.D. glass capillaries (Polymicro Technologies) and sealed with epoxy. The glued capillary was then threaded into1/32"ID x 1/16"OD PTFE tubing (Cole-Palmer) through an extruded hole in the middle of the tubing. The tip of the 0.05 cm I.D. x 0.08 cm O.D. capillary is slightly recessed within the PTFE tubing. A 0.004" I.D. PTFE Special Sub-Light Wall Tubing is then threaded onto the tip of the 0.05 cm I.D. x 0.08 cm O.D. capillary and also encased within the 1/32"ID x 1/16"OD PTFE tubing. Finally, all of the openings are sealed with epoxy, with the end of the 100 µm I.D. x 360 µm O.D. round glass capillary connected to a syringe filled with the aqueous chitosan FePt solution, and the end of the 1/32"ID x 1/16"OD PTFE tubing connected to the oily hexadecane Span 80 solution.

Anisotropic Capsule Preparation. The flow rate of the chitosan dispersed phase is 1 µL/min where as the continuous Span 80-hexandecane phase is 10 µL/min. The droplets are generated in a co-flow microfluidic device then collected in a plastic petri dish containing 2 wt% Span 80 hexadecane. After collection, the petri dish is carefully placed on top of a neodymium magnet for 1 hour until all of the FePt NP are concentrated to a point on the bottom of the chitosan droplet. Then, 2 wt% glutaraldehyde in Span 80 hexadecane solution is carefully added to the petri dish. After approximately 10 min, the

anisotropy is fixed and the petri dish can be removed from the magnet and allowed to further crosslink overnight. Finally, in order to wash the crosslinked chitosan capsules, they are purged with nitrogen gas overnight. They are then washed with decanol and ethanol and resuspended in water.

Image Analysis. Bright-field optical images of patchy capsules and movies were taken with a Nikon Eclipse LV-100 Profilometer Microscope. Capsule sizes (length and radius) were determined using the Nikon Microscope software. Mean speed and distance travelled were analysed using ImageJ's MTrackJ plugin[54,78], averaged over at least 10 s of recorded video.
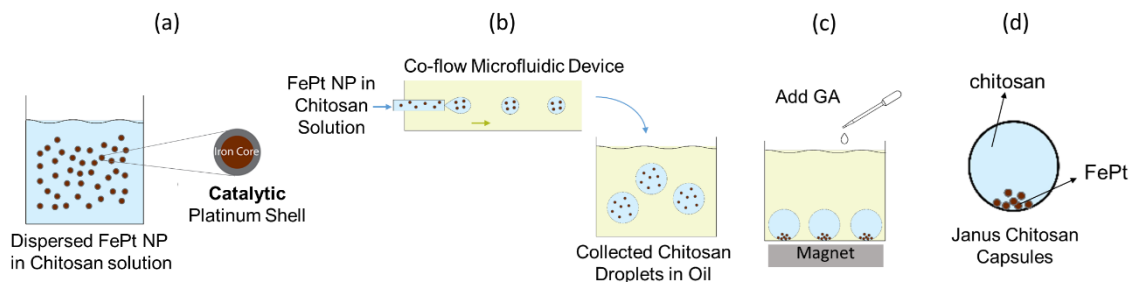
Figure 4.2. Generation of capsules having a patch of FePt NPs. (a) FePt NPs (iron-oxide core and a Pt shell) are initially dispersed in a chitosan solution. Because of the iron oxide core, the particles are attracted to a magnet. (b) the chitosan solution containing FePt is emulsified into an oily phase using a co-flow device built in-house using glass capillaries and PTFE tubing. The chitosan droplets are then collected in a container with the same oily phase; (c) the droplets are then placed on a neodymium magnet for 1 hour so that all of the NPs are pulled to one side of the droplet. Crosslinker (2 wt% glutaraldehyde) is then carefully added to the droplet solution. (d) Within 10 min incubation, the droplets are already fixed into capsules and can be removed from the solution. Further overnight incubation yields densely crosslinked capsules.

4.3. Results and Discussion

We first synthesized FePt NPs that have magnetic and catalytic capabilities, as described above. This involved the thermal decomposition of iron pentacarbonyl ($Fe(CO)_5$) and subsequent reduction of platinum acetylacetonate ($Pt(acac)_2$) in the presence of oleic acid and oleylamine.[77] In addition to being magnetic and catalytic, the core/shell structure provides the benefit of reduced material cost as opposed to using pure Pt nanoparticles. The diameter of the NPs was 84 ± 8 nm by DLS.

The synthesis of patchy capsules containing these NPs is shown in Figure 4.2. We use a capillary co-flow device to make chitosan droplets bearing FePt NPs. First, 0.01 wt% FePt NPs are dispersed in a 2 wt% chitosan solution (Figure 4.2a). This aqueous solution serves as the dispersed phase, and it is sent through the inner capillary of the microfluidic device. The oil phase is hexadecane containing the nonionic surfactant, Span 80 (2 wt%) and it is the outer (continuous) phase injected through the PTFE tubing. Both flow rates are controlled by syringe pumps, with typical flow rates of 10 µL/min (inner) and 1 µL/min (outer) flow. The droplets generated by the microfluidic device are collected in a plastic petri dish, as shown schematically in Figure 4.2b. A photograph of these droplets is shown in Figure 4.3a. The petri dish is placed on top of a neodymium magnet (Figure 4.2c). Within 1 h, all of the FePt NPs are concentrated as a patch at the bottom of each drop (closest to the magnet). (photograph in Figure 4.3b). Glutaraldehyde (GA), a common chemical crosslinker for chitosan, is then added drop wise to the petri dish to permanently fix the magnetically induced anisotropy. After 10 min, the petri dish can be removed from the magnet and the droplets are left to crosslink overnight.
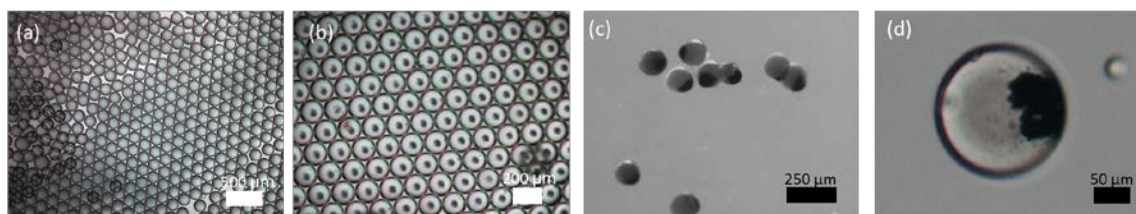
Figure 4.3. Optical micrographs of (a) emulsion of aqueous chitosan droplets bearing FePt NPs; (b) above droplets placed on top of a magnet after 1 h – all the FePt NPs have migrated to a point at the bottom of the droplets; (c) chitosan capsules post crosslinking and washing, redispersed in water; (d) close up image of a chitosan capsule from (c) showing its patchy nature. Scale bars: (a) 500 µm (b) 200 µm, (c) 250 µm, and (d) 50 µm.

The patchy capsules are then washed with decanol and ethanol and redispersed in water. While the surfactant in the oil retards coalescence of the droplets, some coalescence is inevitable during the contact time with the magnet. Therefore, the washed chitosan capsules are filtered using 160 µm Nylon filters to remove any coalesced capsules. The optical micrograph in Figure 4.3c shows that the final capsules are relatively monodisperse and discrete. The closeup in Figure 4.3d reveals the patchy nature of the capsule, with all the NPs collected in a single patch at one end. The above method for preparing patchy capsules is similar to that in recent reports (where the focus was on patchy magnetic particles);[22,79] to our knowledge, this is the first time this method has been coupled with catalytic NPs to make micromotors.

To study the self-propulsion of the micromotors, we placed individual capsules in a petri dish containing a solution of H_2O_2 at a given concentration. All micromotors showed autonomous motion by the mechanism in Figure 4.1 and a series of images showing such motion are provided in Figure 4.4a. Interestingly, four different trajectories were observed for the same batch of micromotors. The majority of the trajectories were either circular or linear. Circular motion in the clockwise and counterclockwise rotation were frequently

45

observed, as were linear trajectories. We also observe the occasional switch between linear and circular motion, but we did not observe alternating trajectories between counterclockwise and clockwise circular motion. The stochastic nature of micromotor trajectories is because its motion is driven by ejected bubbles, and this has been observed elsewhere.[12] Specifically, the initial direction of bubble ejection from the micromotor (or the initial pinned position of the bubble on the micromotor), determines the subsequent path of the micromotor. Note that the patch of FePt NPs inside the capsule can have different orientations, which can dictate the direction of ejected bubbles.
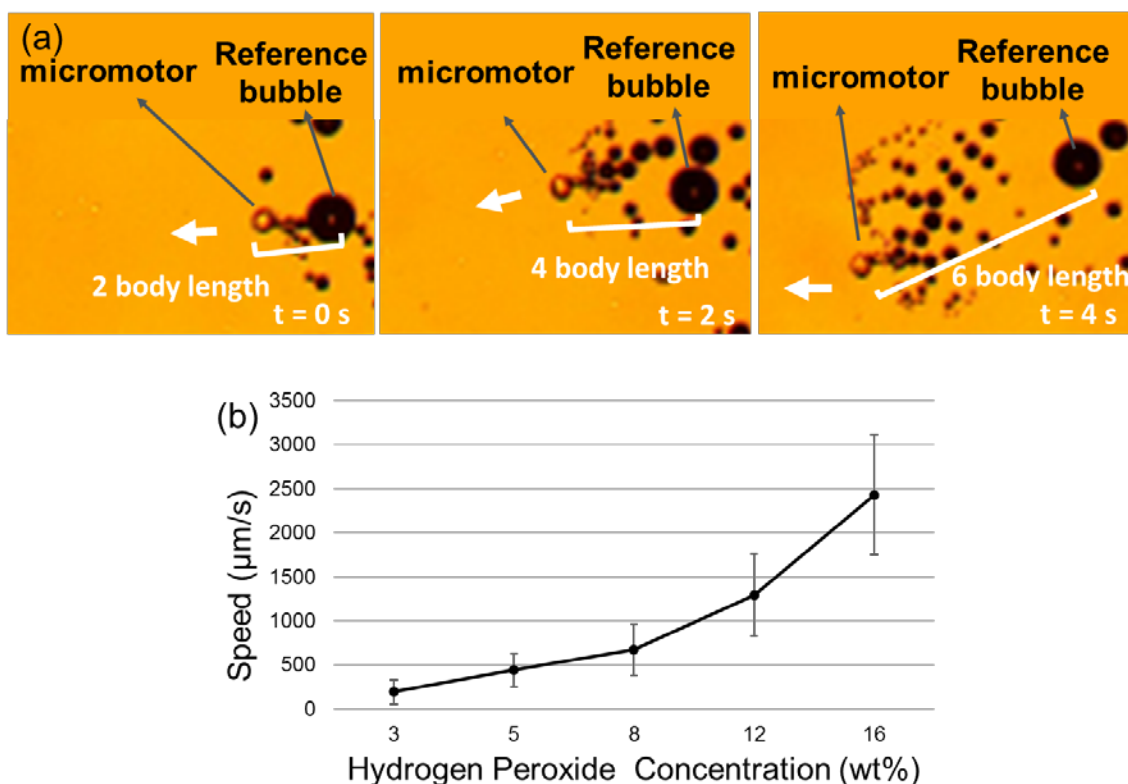
Figure 4.4. Self-propulsion of micromotors in H₂O₂ solution. (a) Images taken from a video demonstrating self-propulsion. (b) Average speed of the micromotors in varying concentrations of H_2O_2. Trajectories of 10 micromotors were sampled at each concentration over a period of 60 s. The error bars are standard deviations of the average speed of the 10 micromotors.

A key parameter that affects self-propulsion is the concentration of H_2O_2. We found a monotonic trend between this concentration and the speed of the micromotors (Figure 4.4b). At the lowest H_2O_2 concentration tested (3%), the speed was ~ 200 µm/s, or ~ 1 body length/s. In contrast, the same capsule is capable of moving at 2400 µm/s, or 10 body lengths/s at the highest H_2O_2 concentration (16%). Thus, a 5-fold increase in H_2O_2 concentration causes the speed to increase by an order of magnitude. The higher speed at higher concentrations visually correlated with an increase in the frequency of oxygen bubble generation.
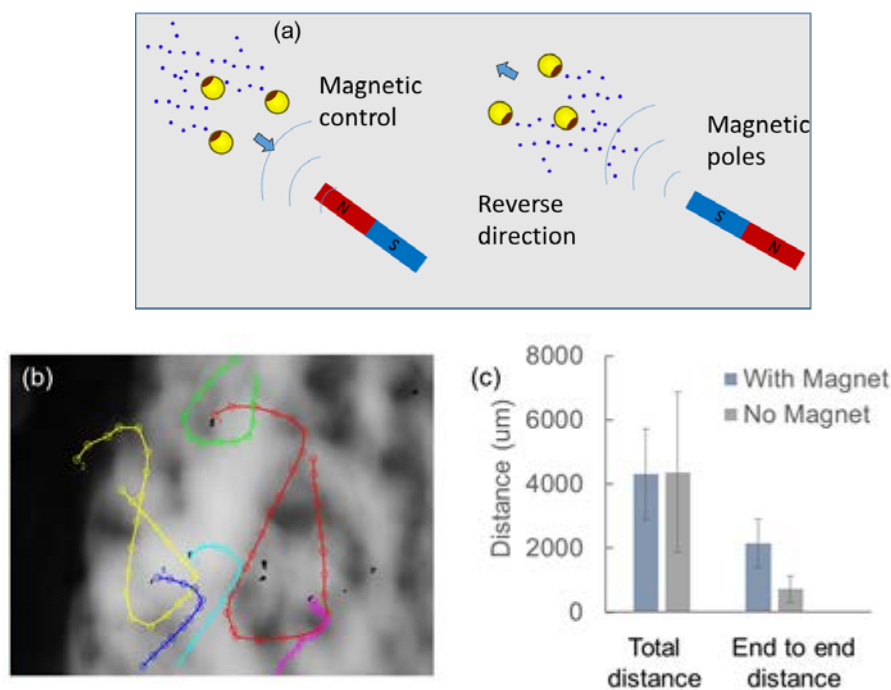
Figure 4.5. Magnetic response of the micromotors. (a) Due to the magnetic nature of the FePt NPs, the micromotors have a permanent magnetic dipole. This is demonstrated by placing a magnet near the self-propelling micromotors, whereupon, all the micromotors collectively move towards the magnet; (b) Collective trajectories of multiple micromotors under the influence of an external magnet; trajectories are drawn with MTrack; (c) The total distance travelled and the end-to-end distance of micromotors in 8% H_2O_2 solution with and without an external magnetic field. The total distance travelled is unchanged (*n*

=5), however, the end-to-end distance is much greater under a magnetic field (p<0.05), indicating an increase in directionality, proving that the micromotor travel in a more linear trajectory. The measured time for all micromotors is the same (6 s, 60 frames).

Due to the ferromagnetic nature of the iron oxide core in the FePt NPs, the micromotors also exhibit sensitivity to a magnetic field (Figure 4.5a). This is demonstrated by placing a permanent magnet near the micromotors that are already moving randomly in an H_2O_2 solution, whereupon, all the micromotors collectively move towards the magnet. When the polarity of the magnet is reversed, the micromotors swim away from the magnet. This indicates that the micromotors have magnetization with defined polarity, either being attracted toward the permanent magnet or being repelled by it. We hypothesize that the reason for the polarity is because during capsule synthesis, the neodymium magnet orients the magnetic domains of the FePt.[10]

Figure 4.5b traces the trajectories of micromotors being controlled by an external magnet. The magnet can be used to change the direction of the micromotors. Some micromotors enter and leave the field of view, but the path taken by the micromotors when in view are moving in unison due to the external magnetic field. To confirm that the micromotors are not moving purely due to magnetic actuation, we measured the total distance travelled for 6 seconds with and without an external magnet, and found that this is nearly the same (Figure 4.5c). On the other hand, the end-to-end distance is significantly higher (3 times, p<0.05) in the presence of the magnet. Similar observations were made in previous studies.[10,51] We conclude that the magnet only provides directionality and does not exert a significant force on the micromotors.

We further demonstrate this magnetized behavior by isolating a micromotor that is moving counterclockwise in the absence of a magnet. Then, when we place the magnet (magnet on), the micromotor starts moving in a linear trajectory toward the magnet (to the right of the microscope, not imaged). Next, the magnet is briefly removed (magnet off), whereupon the micromotor resumes its original counterclockwise motion. Finally, the magnet is placed again with its polarity reversed (magnet on), and the micromotor reverts to a linear trajectory, but in the opposite direction. An additional point is that the micromotor always moves away from the bubbles, i.e., it is the bubble ejection that propels the micromotor forward. Note that the patch of FePt NPs does not face toward the magnet. This substantiates the idea that the magnet does not exert a significant force on the micromotor. The magnet simply allows us to control the trajectory of the micromotor.
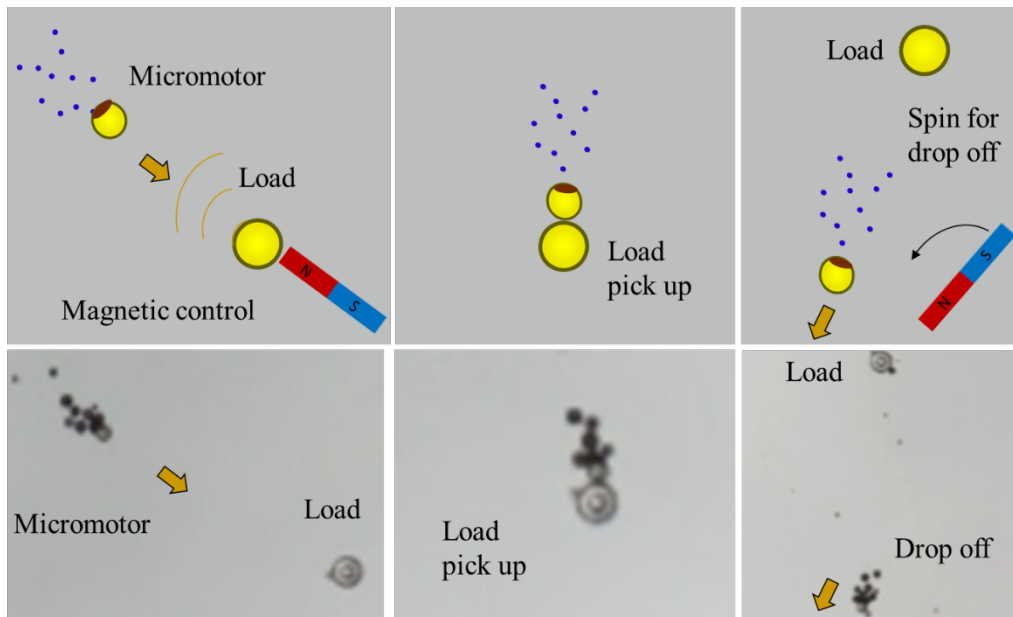
Figure 4.6. Pick up and drop off capability of a micromotor. Under magnetic control, micromotors can travel towards a particular load, which in this case is an empty chitosan capsule. When directed to meet the load head on, the micromotor sticks to the load due to the soft nature of the two. This allows the load to be picked up. After travelling a certain

distance, the micromotor can then drop off the load. This is done by flicking the magnet so that the micromotor can have a sudden change in direction.

Being able to magnetically control the micromotor allows them to be used for directional maneuvering and target pick up. Because chitosan capsules are soft materials, we found that they have an inherent tendency to stick to one another when they come into contact. We use this to demonstrate the ability of our micromotor, under the control of an external magnet, to pick up another chitosan capsule (with no FePt NP), shown in Figure 4.6 (a), traversing a distance (b) with the plain chitosan capsule before the micromotor drops off the chitosan capsule (c). We achieve the drop off by flicking the magnet in the opposite direction of the micromotor's path to induce a "slide off" from the chitosan capsule cargo.

4.4. Conclusions

We have demonstrated the ability to create a chitosan based microswimmer that is capable of self-propelled motion in a hydrogen peroxide solution. These anisotropic micromotor capsules are capable of generating oxygen due to the platinum in the nanoparticles catalysing the reaction of hydrogen peroxide to water and oxygen. At different concentrations of hydrogen peroxide, the rate of bubble production, or speed of the overall microswimmer, increases with increasing hydrogen peroxide. The direction of the microswimmer can also be controlled by a magnet. During the crosslinking process, the polarity of the nanoparticles becomes fixed. This allows us to control the direction of the microswimmer by changing the rotation of the magnet, instead of physically placing the magnet at the desired location. We have also demonstrated the possibility of picking up another soft material and transporting it a certain distance before dropping it off. Overall,

we have put forward a new method for creating a biopolymer based microswimmer that is capable of all the aforementioned traits found in its predecessors. An attractive feature of this method is that the micromotors are biodegradable and can be potentially used in applications such as environmental clean-up and decontamination.

Chapter 5

Multicompartment Capsules and Their Use to Study Bacterial Signaling

5.1. Introduction

Containers with separated inner compartments that can perform simultaneous or cascade reactions, while keeping encapsulated reactants separated from the products freely diffusing in the same environment, is extremely attractive for applications of catalysis,[80-83] drug delivery,[84,85] and tissue engineering.[86-89] Such multicompartment containers on the micron scale are considered artificial cells, due to the overall structure being similar to organelles enclosed in discrete, functional membranes within the cell. Much similar to the cell, multicompartment containers should be aqueous, with the internal structures separated by membranes that allow transport of small molecules. The concept of artificial cells have long existed in the realm of therapeutic cell culture and tissue engineering.[86,87,89] On the simplest scale, an artificial cell is merely an encapsulation scheme used to protect the enclosed materials from the external environment.[86] Typical approaches to making multicompartment structure have either used inhomogeneous phase emulsions, such as in double emulsion methods,[90] or using layer-by-layer techniques[81,84,91] to create multilayer shells around a core capsule. In tissue engineering, it is common to further protect the encapsulated material with a second bounding layer to prevent any contact of the internal encapsulants from the external environment.[86] Recently polymerosomes and liposomes have been encapsulated[80,82,83,92] in larger containing capsules through self-assembly, which provide a promising step toward synthetic cell containers and have demonstrated possibilities of enzymatic cascade reactions. However, no system have demonstrated the ability to use microfluidics to create multicompartment capsules with controlled size and

shape, and most importantly, with a purely aqueous, biocompatible system. Here, we conceptualize our vision toward an artificial cell like multicompartment capsule by using alginate in a two-step microfluidic process.

Our multicompartment capsule, in its entirety, consist of the negatively charged polyelectrolyte alginate. Using polysaccharides such as alginate is advantageous due to the many positive attributes of the biopolymer, such as biocompatibility, low toxicity, simple capsule formation, and ease of complexation with other positively charged polysaccharides to form bounding membranes. The bounding membrane in our capsule is formed by electrostatic complexation with the positively charged polyelectrolyte chitosan, and the membrane is the only separation between the inner compartments and the bounding capsule. Similar to the nuclear envelope, the polyelectrolyte shell keeps the encapsulated material in place while still allowing small molecules to diffuse freely between the membranes.[87,92,93] The flexible shell formed between the two oppositely charged polymers has been shown to act as a cytoprotective layer[94] and reduce bacterial leakage,[95] while the inner alginate matrix have been reported to encapsulate a variety of biological materials, such as enzymes,[82,83] adsorbents,[96] tissues,[89] islets,[86] bacterial cells.[65,90,97]

The novelty in our multicompartment capsule is that we employ a microfluidic pulsed air technique to generate our alginate capsules. Microfluidically generated capsules have sizes that can be easily controlled by changing two parameters, syringe pump flow rate and pulse frequency. Using microfluidics to control the size and shape of the microencapsulated environment has shown new interesting behaviors for mammalian and

bacterial cells.[98-100] In particular, microencapsulation of bacteria has led to new understanding of the way bacteria regulate quorum sensing.[98,101] Quorum sensing is a density dependent cell behavior that allows bacteria to use small diffusible molecules, such as autoinducers, to communicate with neighboring bacteria. Using microenvironments to study quorum sensing between bacteria has taught us unexpected behaviors. For example, single bacteria can exhibit quorum sensing phenotypes when encapsulated in a small droplet.[102] Sender and receiver systems have also been encapsulated in droplet emulsions and show that quorum sensing molecules can diffuse from a reservoir droplet to turn on bacteria encapsulated in neighboring droplets.[97] Here, we show that our multicompartment capsule can encapsulate AI-2 producer and genetically engineered reporter bacteria in the inner compartments. AI-2 producer bacteria can produce autoinducer-2 (AI-2), a quorum sensing molecule that is associated with nearly 70 different species of bacterial, many of which are pathogenic. The AI-2 producer BL21(LuxS+) strain overproduces AI-2 molecules, thereby increases the concentration of the AI-2 in the microenvironment. Once the reporter cells senses the AI-2, the cells turn on the gene to produce a fluorescent protein, which can be observed microscopically. We believe our system is not only useful to study quorum sensing between bacteria, but also present an opportunity to bring two un-coinhabitable organisms into one microenvironment. This encapsulation scheme can be used to further explore cross kingdom communication or co-culturing of competitive species.
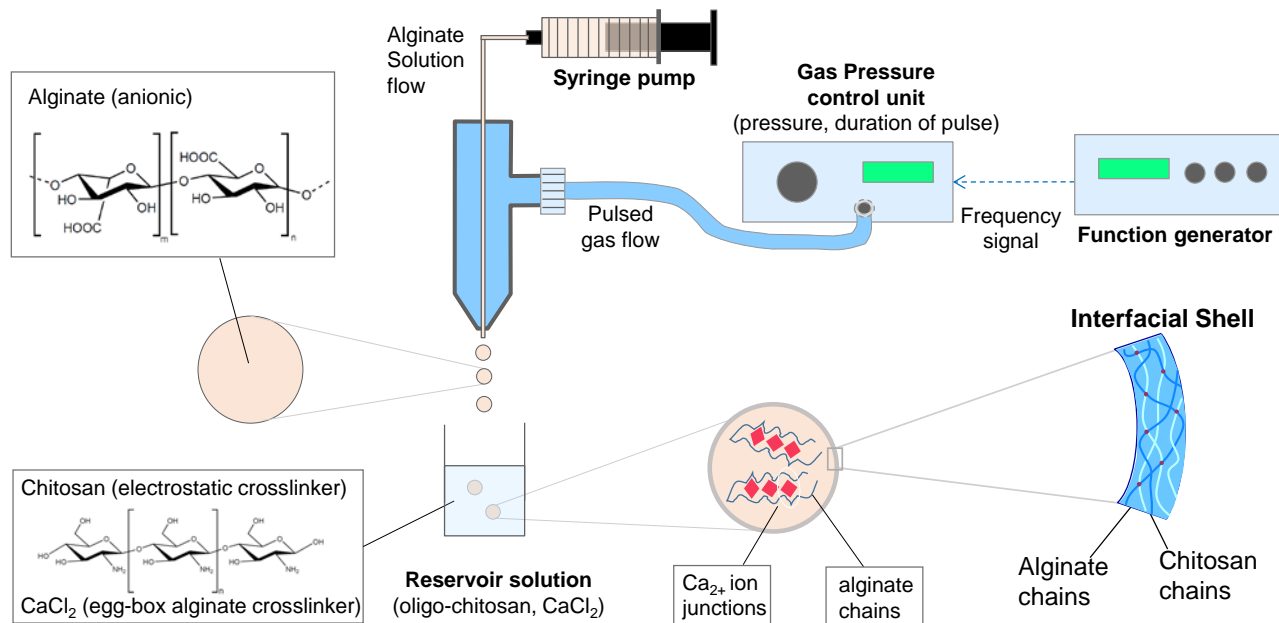
Figure 5.1. Schematic of pulsed air flow droplet generation system. Alginate solution is injected by a syringe at a flow rate controlled by a syringe pump. A pulsed gas is generated by the function generator and the gas pressure is adjusted by the pressure control unit. Alginate droplets are generated by the pulsed gas flow and collected in a reservoir solution containing oligo-chitosan, calcium chloride, and surfactant. Chitosan forms shell with alginate due to electrostatic interactions and the calcium forms egg-box junctions with alginate core, forming a crosslinked network.

5.2. Experimental Section

Materials and Chemicals. Alginate (alginic acid sodium salt from brown algae; medium viscosity), calcium chloride dihydrate, chitosan oligosaccharide lactate (low molecular weight chitosan, M_n~5,000; degree of deacetylation > 90%), the nonionic surfactant, Pluronic F-127, were obtained from Sigma-Aldrich. 1x PBS (Dulbecco's phosphate-buffered saline; no calcium, magnesium, phenol red), 1x LB broth, were obtained from Life Technologies and used without further modifications. Water soluble magnetic nanoparticles (EMG 304, 10 nm) was purchased from Ferrotec and diluted 10x with 1x

PBS. Fluorescently labeled green and red capsules (0.7-0.9 µm, 1.0% w/v) was purchased from Spherotech and used without further modifications.

Solution Preparation. Stock solution of 1 wt% and 4 wt% alginate was dissolved in 1x PBS and filtered with 0.45 µm Millipore Cellulose Syringe Filters. For non-cell encapsulated droplet generation, 0.4 g of 1 wt% alginate solution, 0.4 g of EMG 304 dilution, and 0.2 g of fluorescently labeled capsules was added to 1 g of 4 wt% alginate solution to yield a final concentration of 2.2 wt% alginic acid. For cell encapsulated droplet generation, 0.5 g of 1 wt% alginate was added to 0.5 g of the cell pellet and then added to 1 g of 4 wt% alginate to yield a final concentration of 2.25 wt% alginic acid. Reservoir solution consist of 1 wt% chitosan oligosaccharide lactate, 1 wt% calcium chloride dehydrate, and 0.3 wt% Pluronic F-127.

Device Fabrication. Droplet generation device is fabricated in-house and show in Figure 2.7. 0.5" of a severed seven barrel glass capillary (World Precision Instruments) is inserted into the male of the Luer adapter tee (Cole-Parmer, EW-45508-85). 0.5" of a hydrophobically modified 50 µm inner diameter (ID) glass capillary (Vitrocom, CV0508) is threaded and epoxied into a 50 mm 200 µm ID square capillary (Vitrocom, 8320). The square capillary is then inserted into the center of the multibarrel capillary. The extruded square capillary on the side of the female connector is then inserted and epoxied into a piece of tygon tubing (Cole Parmer, EW-06509-13). A male luer syringe connector with 1/16" hose barb is then inserted into the tygon tubing (Cole Parmer, EW-45518-00), with the exposed male luer capable of connecting to any female syringe. A P1000 plastic pipette

56

is cut to encase around the capillary apparatus to focus the gas stream, then sealed with epoxy.

Image Analysis. Bright-light field images and fluorescence microscopy was performed with MVX10 MacroView fluorescence stereomicroscope (Olympus, Center Valley, PA) equipped with a DP72 Camera. Images were taken with FITC and TRITC filter sets and were overlaid using the Adobe Photoshop to visualize both colors simultaneously.

Cell culture. Two types of e. coli reporter strains were used: W3110 ($\Delta luxS$) + pCT6 + pET-dsRed for red fluorescent expression and W3110 ($\Delta luxS$, $\Delta lsrFG$) + pCT6 + pET-GFPuv for green fluorescent expression. BL21 (LuxS+) was used as AI-2 producers, and W3110 ($\Delta luxS$, $\Delta lsrFG$) + pCT6 + pET-Venus was used as reporters of AI-2. Plasmid constructs are described by Tsao et al. All E.coli strains were grown in LB medium; W3110 ($\Delta luxS$, $\Delta lsrFG$) + pCT6 + pET-Venus was supplemented with kanamycin and ampicillin (50 µg mL^{-1} per antibiotic) at 37C and 250 rpm until an optical density (at 600 nm) of 0.4 was reached. Subsequently, cultures were centrifuged at 3,900 rpm for 7 min and resuspended in 0.5 g of 1x PBS. The final concentration of the E.coli in the alginate suspension is the same as initial E.coli concentration in the LB medium. Once encapsulated, the capsules are shaken at 37C to fully express the fluorescent protein VENUS.

Chapter 5.3. Results and Discussion
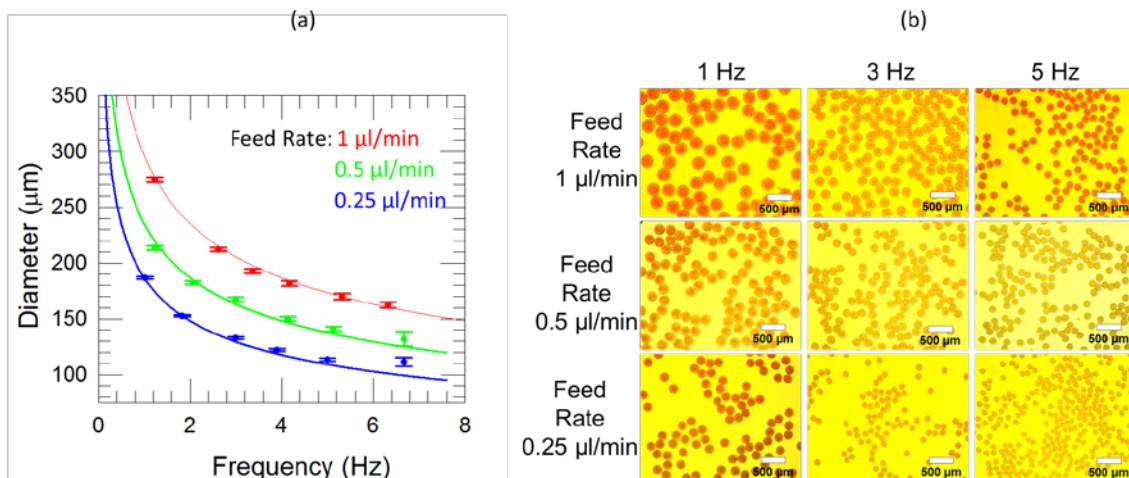
Figure 5.2. (a) Alginate droplets are generated using the gas pulse generator at 1 Hz to 7 Hz and at syringe pump flow rates from 1 ul/min to 0.25 ul/min. Capsule diameter decreases with increasing frequency and decreasing flow rate, portrayed by estimated and experimental results. Capsules generated at 7 Hz are no longer 1 per pulse. (b) Image of collected capsules at different gas pulse generator frequency and different syringe pump flow rate.

The first component of our double encapsulation scheme is to create the smaller alginate capsules that serve as the inner compartments of our multicompartment capsule. Starting with our homemade microfluidic droplet generator (Figure 5.1, Supplemental for device setup), we feed a 2.5 wt% filtered alginate solution using a syringe pump and droplets are generated at the tip of our droplet generator. A pulsing compressed air stream envelops the tip of the droplet generator and impinges and dislodges one droplet at every pulse. The droplets are then collected in a reservoir solution composed of 1 wt% oligochitosan, 1 wt% $CaCl_2$, and 0.3 wt% Pluronic F-127. The positively charged chitosan forms a thin shell on the negatively charged alginate capsule through electrostatic interactions, while the calcium ions quickly diffuse into the alginate core and forms a capsule through the egg-box junction crosslinking. The nonionic surfactant F-127 prevents

aggregation and coalescence of the capsules once in the reservoir. Because of the microfluidic nature of the droplet generation scheme, our capsules are extremely monodispersed, with droplet size variation <2 μm. Once the alginate capsules are made, they are washed with PBS three times and resuspended in PBS.
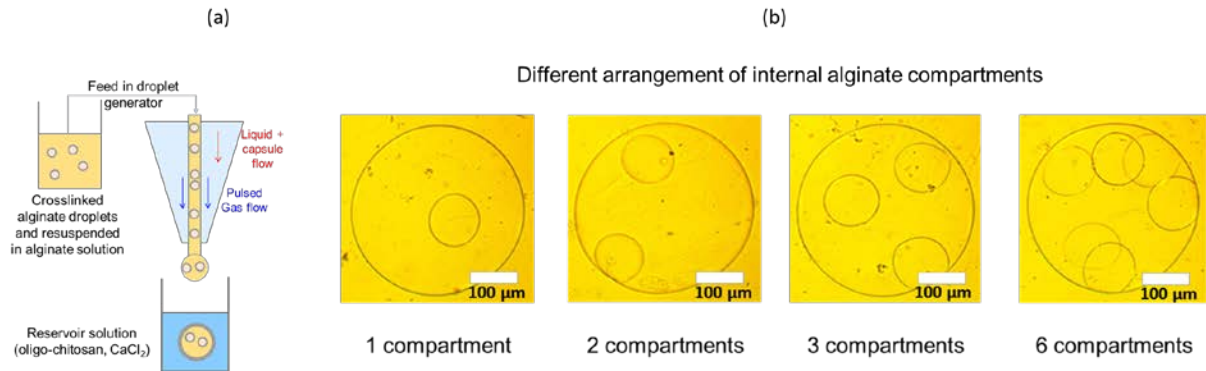
Figure 5.3. Schematic of multicompartment capsule generation process. (a) Alginate capsules are washed and resuspended in alginate solution. This capsule suspension is then injected into a device with a larger diameter tip. Droplets from this device are collected in the reservoir solution. (b) Microscopic images of multicompartment capsules with different arrangement of internal alginate compartment.

The size of the alginate capsules are controlled by two key parameters: flow rate of the syringe pump and the frequency of the function generator, which controls the frequency of the air pulse generated per second and therefore the number of droplets generated per second. The droplet generation frequency can be controlled by the function generator and is varied from 1 to 7 hertz in our experiments. As seen in Figure 5.2, as the frequency of the function generator is increased, the size of the droplets is decreased. An estimation of the droplet diameter can be made by calculating the volume of alginate ejected by the syringe pump (feed flow rate), and divide by the number of droplets generated per second. With Vol_{drop} = *(feed flow rate) x 1/freq* and equating $Vol_{capsule} = Vol_{drop} \times$

$(shrinking\ factor = 0.81)$, we can set diameter of the capsules to $Dia_{capsule} = (6Vol_{capsule}/\pi)^{1/3}$, which provides a relationship of flow rate of the syringe pump to the estimated capsule size. We find that the estimated capsule size from our calculations closely match our experimental results, except at high pulse frequencies. At frequencies past 6 Hz, droplets were no longer generated one per pulse, yielding capsules with a large size distribution. It should be mentioned here that the pulse generator in our schematic (Fig 1) controls the air pressure that is used to dislodge the droplet forming at the tip of the hydrophobically modified glass capillary, and can be adjusted accordingly. However, once tuned to the right pressure, it is not changed further to affect the size of the droplets.

The second part to our multicompartment capsules is to re-encapsulate the smaller alginate capsules. This is accomplished by adding alginate to the washed alginate capsules suspended in PBS to a final 2.2 wt% alginate solution. This technique of double encapsulation has previously been used to prevent any contact of the encapsulated cells from the external environment. A larger diameter droplet generator is used to ensure that the smaller alginate capsules can flow freely without clogging the device. We typically use a hydrophobically modified 300 µm capillary for the second encapsulating process. The droplet generation scheme is repeated as in Figure 5.3(a) and the desired multicompartment capsule can be picked out with a pipette for visualization. Because the internal arrangement of each capsule is random, the resulting multicompartment capsules have a variety of different arrangement of internal alginate compartments. We show several arrangements in Figure 5.3(b). Despite not being able to control the arrangement of each capsule, our

device effectively mixes the inner compartments and we are able to combine more than one type of inner capsule in our multicomparment capsule.

The flexibility of the two step encapsulation process gives us great control on how we want the morphology of the internal compartments to look like. Two different species of biologics encapsulated in smaller alginate capsules can be incorporated into the larger alginate capsule to maximize the function of our design. Because alginate is a biocompatible polymer commonly used to encapsulate a variety of components, we have chosen to demonstrate the utility of our multicompartment capsules first by encapsulating green and red fluorescent capsules, seen in Figure 5.4(a). Two alginate solutions were separately prepared, where we loaded each with green and red fluorescent capsules. Each type of red and green alginate capsules were first generated, washed, and then combined to make the 2.2 wt% alginate solution that will be injected into the larger diameter device, with resulting capsules shown in top row of Figure 4. We repeat the same procedure for encapsulating two strains of bacterial cells, as seen in Figure 5.4(b). We demonstrate the concept of culturing two genetically engineered reporter bacterial strains, W3110 (ΔluxS) + pCT6 + pET-dsRed for red fluorescent expression and W3110 (ΔluxS, ΔlsrFG) + pCT6 + pET-GFPuv for green fluorescent expression. The strains are typically used to detect and respond fluorescently to the quorum sensing molecule, AI-2. However, the bacteria are luxS mutants, meaning they cannot synthesize their own AI-2. LuxS converts S-ribosylhomocysteine (SRH, a precursor of AI-2) to homocysteine and 4,5-dihydroxy-2,3-pentanedione (DPD); DPD can then spontaneously cyclize to active AI-2. Without luxS, E.coli can only sense AI-2 being produced elsewhere. Fluorescence of both strains were

61

induced with synthetically produced AI-2. We demonstrate that both populations of bacteria can be successfully encapsulated within the same environment but remains separated from contact. If supplemented with LB media and shaken at 37, the encapsulated bacteria eventually forms colonies within the multicompartment capsule, using the alginate matrix as support.
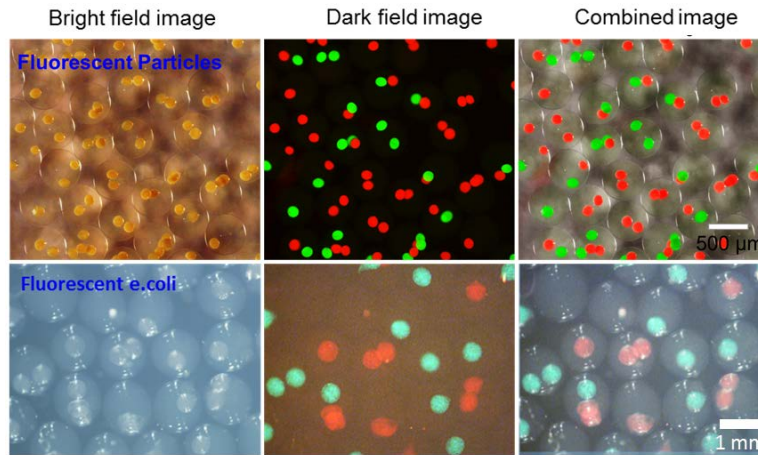
Figure 5.4. Top row: different microscopic images of multicompartment capsules with internal alginate compartments that contain green and yellow fluorescent particles. Bottom row: different microscopic images of multicompartment capsules with encapsulated reporter E.coli. Two types of E. coli reporter strains were used: W3110 (Δ*luxS*) + pCT6 + pET-dsRed for red fluorescent expression and W3110 (Δ*luxS*, Δ*lsrFG*) + pCT6 + pET-GFPuv for green fluorescent expression. Both strains were synthetically induced by artificially produced AI-2 to express their fluorescent proteins.

Quorum sensing is an important process in bacterial communication that changes the phenotype of an entire population. We hypothesize that because our multicompartment capsules allow small molecules to diffuse freely, AI-2 produced from one internal compartment can control the behavior of bacteria in a different compartment. We encapsulate AI-2 producer E.coli and genetically engineered receiver bacterial system in our multicompartment capsule to demonstrate the possibility of using our capsules to study

quorum sensing between two different strains of bacteria, portrayed in the schematic in Figure 5.5 (top left). Here we encapsulate E.coli BL21 (luxS+) and W3110 ($\Delta luxS$, $\Delta lsrFG$) + pCT6 + pET-Venus in our small alginate capsules. BL21 (luxS+) overproduces AI-2. AI-2 responsive e. coli strain, W3110 ($\Delta luxS$, $\Delta lsrFG$) + pCT6 + pET-Venus, was used to detect AI-2 in the environment. This strain responds to a significantly lower AI-2 concentration than wild type W3110 and does not synthesize its own AI-2 (luxS mutant), but produces a fluorescent protein Venus in response to AI-2. VENUS is a yellow fluorescent protein (VENUS) shown green due to the filter settings on our fluorescent microscope. For identifying purposes, we encapsulated the reporter strain in a slightly larger diameter alginate capsule than the producer strain of E.coli; this allowed us to quickly identify the identity of the internal compartments before the sensing event began.

The multicompartment capsules are then placed in LB media for 24 hours, shaken at 37. After 24 hours, we examine the capsules and find that the bacteria have formed colonies within the internal capsules, and the capsules with reporter bacteria is brightly fluorescent, whereas the capsules containing BL21 sender bacteria are dark, in Figure 5.5 (bottom). The background adjusted fluorescent intensity is measured and shown in Figure 5.5 (top right), where fluorescent intensity of the reporter capsules are statistically higher than the fluorescent intensity of the producer capsules. We present a small sample population of the different combination of inner compartments in Figure 5.5 (bottom). The colonies in the outer encapsulating alginate are bacteria that either contaminated the

alginate solution before it was encapsulated or bacteria that leaked during the incubation process and formed its own separate colonies.
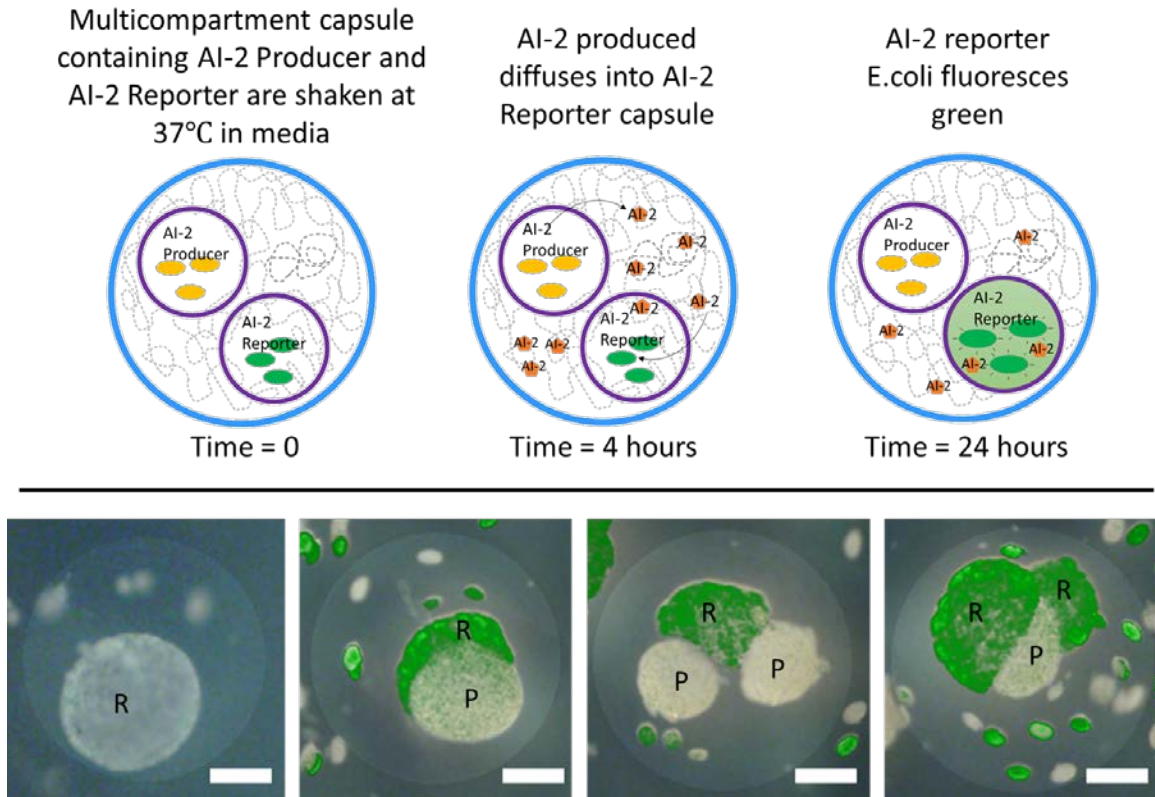
Figure 5.5. Quorum sensing scheme of AI-2 producer and reporter (top left) AI-2 producer E.coli is encapsulated in one set of alginate capsules while AI-2 reporter E.coli is encapsulated in a different set of alginate capsules. When combined into a multicompartment capsule, the AI-2 producer produces AI-2 that diffuses into the compartment, where AI-2 is sensed by the AI-2 reporter strain. After 24 hours, the AI-2 reporter strain expresses the VENUS protein, which causes the entire capsule containing the AI-2 reporter strain to fluoresce green. Top right: fluorescent intensity of Bottom: Different combination of internal compartments of the multicompartment capsule encapsulating AI-2 producer (P) and AI-2 reporter (R) strains of bacteria. Scale bar represent 250 µm.

5.4. Conclusions

We have demonstrated the ability to create alginate based multicompartment capsules that have discrete, controllable, biocompatible inner compartments that are capable of encapsulating AI-2 producer and reporter bacterial strains. The encapsulated

bacteria can form colonies within 24 hours in their alginate microenvironment and secrete and detect quorum sensing molecules. Our method involves a two-step process which allows us the flexibility to load different components into the solution before capsule formation. This is the first time aqueous based multicompartment capsules have been made and used for bacterial communication. We believe our system is capable of studying quorum sensing of bacterial population that are unfavorable to co-culturing environments, and plan to study cross kingdom quorum sensing using our multicompartment capsules

Chapter 6

Conclusions and Recommendations

6.1. Project Summary and Principal Contributions

In this dissertation, we have shown three different kinds of anisotropic microcapsules. These microcapsules were developed by adapting three different microfluidic platforms to create three different genres of anisotropy, i.e. shape anisotropic dimer microcapsules in chapter 3, surface/Janus anisotropic microcapsules in chapter 4, and multicompartment volume anisotropy in chapter 5. These microcapsules were imparted with different functionalities, such as magnetic micro stir bar for dimer microcapsules, self-propelled micromotors for Janus anisotropic microcapsules, and bacterial encapsulation and quorum sensing for multicompartment capsules.

In Chapter 3, we describe the micromanufacturing of Janus-like dimer chitosan microcapsules. These microcapsules were created by bringing two droplets together through coalescence and binding them using chemical crosslinking. This is the first time chemical crosslinking (vs. UV crosslinking) has been used to make anisotropic capsules in microfluidics. Magnetic nanoparticles were embedded in one lobe of the microcapsules to give them properties of magnetic anisotropy so they can rotate when placed on top of a rotating magnetic field.

In Chapter 4, we reported a simple process for inducing anisotropy in a microcapsule. We synthesized magnetic and catalytic nanoparticles to be encapsulated in

the soluble chitosan solution. The chitosan solution was then emulsified into droplets using a microfluidic device. These droplets are then incubated on top of a magnet to localize all of the magnetic nanoparticles. Chemical crosslinking is used to permanently fix the anisotropy of the microcapsules. These microcapsules can self-propel in hydrogen peroxide and respond to magnetic force in hydrogen peroxide. The process for synthesizing the self-propelled micromotors can replace current methods that require metal deposition techniques. Furthermore, the chitosan based micromotors are biodegradable, and can be explored for environmental remediation.

In Chapter 5, we use a gas microfluidic system to create alginate multicompartment capsules. The multicompartment capsules have alginate inner compartments enveloped by an alginate outer capsule. The multicompartment capsules were used to encapsulate E.coli that was capable of communicating with eachother through secretion and detection of the small molecule, autoindcuer-2 (AI-2). The multicompartment capsules demonstrate the first purely aqueous microfluidic encapsulation technique. The capsules can be further explored for studying how biological materials interact through small molecules in a microenvironemt.

We believe the introduction of these microfluidic platforms for generation of anisotropic microcapsules will find a wide range of applications.

6.2. Recommendations for Future Work

The concepts that we have reported in this dissertation can be extended to explore and envision new applications and utilities. Here, we briefly describe the outline for the future work.

6.2.1 Multicompartment Capsules

In chapter 5, we describe multicompartment capsules which can encapsulate different strains of bacteria in its inner compartments. Bacteria encapsulated in one container can secret small molecules that diffuse to another container in the same capsule. However, it was visible that bacteria from the inner compartments can leak from the inner compartments and colonize in the outer membrane of the capsule. Cell leakage from alginate capsules have been previously reported.[86,89,103] Many researchers have tried to reduce cell leakage by coating the alginate capsules with the addition of a cytoprotective membrane, such as oppositely charged chitosan,[94] polydopamine,[103] and also alginate itself[86]. The most common approach is to complex the negatively charged alginate with positively charged chitosan to form an electrostatic membrane. This membrane has been reported to reduce cell leakage of yeast cells[104]compared to regular alginate capsules. We have replicated the electrostatic complexation to in our multicompartment capsules, but singular bacteria can still leak and colonize the external membrane.

Figure 6.1. Multicompartment capsules made with alginate inner capsules with iron nanoparticles and chitosan/SDBS outer capsules. (a) chitosan capsules formed by complex coacervation with SDBS. (b) alginate capsules formed by coacervation with chitosan and calcium chloride. Magnetic nanoparticles were dispersed within the alginate capsules for separation and imaging. (c) multicompartment capsules made with alginate inner capsules and chitosan outer capsule.

As an alternative to using alginate in alginate multicompartment capsules, we propose a similar system that uses alginate as the inner compartments and chitosan as the outer containing capsule. By introducing chitosan as the outer containing capsule rather than just the membrane between the inner and outer compartments, we believe bacterial leakage as well as bacterial viability in the outer membrane will be greatly reduced due to the antibacterial properties of chitosan. Chitosan can form capsules by simple coacervation with a negatively charged surfactant. Typically, Sodium dodecylbenzenesulfonate (SDBS) or Sodium Triphosphate (TPP) are used to form chitosan capsules. However, since TPP is a strong calcium chelator due to its three negatively charged phosphate groups, we chose the surfactant SDBS for our coacervation system. The multicompartment capsules made with alginate inner capsules and chitosan/SDBS outer capsules. (a) Chitosan capsules formed by complex coacervation with SDBS. Various concentrations of SDBS were tested. 1-4 wt% SDBS resulted in soft capsules that eventually collapsed on itself. 5 wt% SDBS yielded the most robust capsules. Long term storage in SDBS (>20 min) resulted in

shriveling of the capsules. Stable capsules were formed after the chitosan turned a translucent white color, shown in above image. (b) Alginate capsules formed by coacervation with chitosan and calcium chloride. Magnetic iron nanoparticles were dispersed within the alginate capsules for separation and imaging. (c) Multicompartment capsules made with alginate inner capsules and a chitosan outer capsule. Long term storage in SDBS resulted in shrinking of both the inner and outer capsules.

We demonstrate the possibility of macroscale alginate and chitosan multicompartment capsules. However, two preliminary experiments must be performed. We propose using the same micro-dropper used in chapter 5 to reduce the size of our capsules. Bacteria viability must be tested in both the macroscale capsules as well in the microscale multicompartment capsules. Electrostatic interaction between the chitosan shell and bacteria could become a larger problem on cell viability since it is undetermined whether the antibacterial properties of chitosan is a result of electrostatic interactions (bacteria are typically negatively charged) or a physiological interaction(killing through contact).

6.2.2 Automated control of micromotors

In chapter 4 we describe the synthesis of micromtors by inducing anisotropy of the disbursed FePT NP. Micromotors are capable of self-propelled movement through the reaction between platinum and hydrogen peroxide. The generated oxygen bubbles are used to drive the micromotor forward. Studies have shown that zinc in acidic environments can produce similar hydrogen bubbles for bubble propelled motion. Nanoparticles composed

of zinc and iron oxide (Zn/Fe) have been reported in literature. We believe that by using our two step method to induce anisotropy, micromotors with the ability to react with zinc can be synthesized. Such micromotors have been theorized for drug delivery in acidic environments, such as low pH environments like the human stomach.

Additional work has been proposed to automatize controlling micromotor direction. We have demonstrated that micromotors can be controlled with an external magnet. Magnetic rotation can also be automated by using a computer controlled software and a turning platform, such as an Arduino system. Arduino systems can be programmed to turn in simple circular directions. With an attached magnet, we show that Arduinos can be used to control the direction of the micromotor, without human manipulation. We believe with image tracking that feeds back information to the ardruino, the micromotor trajectory can be controlled with more precision.

REFERENCES

[1]   de Gennes, P. G. "Soft matter." *Reviews of Modern Physics* **1992**, *64*, 645-648.

[2]   Comiskey, B.; Albert, J. D.; Yoshizawa, H.; Jacobson, J. "An electrophoretic ink for all-printed reflective electronic displays." *Nature* **1998**, *394*, 253-255.

[3]   Gratton, S. E. A.; Ropp, P. A.; Pohlhaus, P. D.; Luft, J. C.; Madden, V. J.; Napier, M. E.; DeSimone, J. M. "The effect of particle design on cellular internalization pathways." *Proceedings of the National Academy of Sciences* **2008**, *105*, 11613-11618.

[4]   Wu, Y.; Lin, X.; Wu, Z.; Möhwald, H.; He, Q. "Self-Propelled Polymer Multilayer Janus Capsules for Effective Drug Delivery and Light-Triggered Release." *ACS Applied Materials & Interfaces* **2014**, *6*, 10476-10481.

[5]   Wu, Z. G.; Wu, Y. J.; He, W. P.; Lin, X. K.; Sun, J. M.; He, Q. "Self-Propelled Polymer-Based Multilayer Nanorockets for Transportation and Drug Release." *Angewandte Chemie-International Edition* **2013**, *52*, 7000-7003.

[6]   Appleyard, D. C.; Chapin, S. C.; Srinivas, R. L.; Doyle, P. S. "Bar-coded hydrogel microparticles for protein detection: synthesis, assay and scanning." *Nature Protocols* **2011**, *6*, 1761-1774.

[7]   Kagan, D.; Calvo-Marzal, P.; Balasubramanian, S.; Sattayasamitsathit, S.; Manesh, K. M.; Flechsig, G.-U.; Wang, J. "Chemical Sensing Based on Catalytic Nanomotors: Motion-Based Detection of Trace Silver." *Journal of the American Chemical Society* **2009**, *131*, 12082-12083.

[8]   Valadares, L. F.; Tao, Y. G.; Zacharia, N. S.; Kitaev, V.; Galembeck, F.; Kapral, R.; Ozin, G. A. "Catalytic nanomotors: self-propelled sphere dimers." *Small* **2010**, *6*, 565-72.

[9]   Solovev, A. A.; Sanchez, S.; Pumera, M.; Mei, Y. F.; Schmidt, O. G. "Magnetic Control of Tubular Catalytic Microbots for the Transport, Assembly, and Delivery of Micro-objects." *Advanced Functional Materials* **2010**, *20*, 2430-2435.

[10]   Zhao, G. J.; Sanchez, S.; Schmidt, O. G.; Pumera, M. "Micromotors with built-in compasses." *Chemical Communications* **2012**, *48*, 10090-10092.

[11]   Wheat, P. M.; Marine, N. A.; Moran, J. L.; Posner, J. D. "Rapid Fabrication of Bimetallic Spherical Motors." *Langmuir* **2010**, *26*, 13052-13055.

[12]   Wang, S.; Wu, N. "Selecting the swimming mechanisms of colloidal particles: bubble propulsion versus self-diffusiophoresis." *Langmuir* **2014**, *30*, 3477-86.

[13]   Manesh, K. M.; Cardona, M.; Yuan, R.; Clark, M.; Kagan, D.; Balasubramanian, S.; Wang, J. "Template-Assisted Fabrication of Salt-Independent Catalytic Tubular Microengines." *Acs Nano* **2010**, *4*, 1799-1804.

[14]   Glotzer, S. C.; Solomon, M. J. "Anisotropy of building blocks and their assembly into complex structures." *Nature Materials* **2007**, *6*, 557-62.

[15]   Park, J. G.; Forster, J. D.; Dufresne, E. R. "High-yield synthesis of monodisperse dumbbell-shaped polymer nanoparticles." *Journal of the American Chemical Society* **2010**, *132*, 5960-+.

[16]   Jiang, S.; Chen, Q.; Tripathy, M.; Luijten, E.; Schweizer, K. S.; Granick, S. "Janus particle synthesis and assembly." *Advanced Materials* **2010**, *22*, 1060-1071.

[17]   Lee, K. J.; Yoon, J.; Lahann, J. "Recent advances with anisotropic particles." *Current Opinion in Colloid & Interface Science* **2011**, *16*, 195-202.

[18]   Hong, L.; Jiang, S.; Granick, S. "Simple method to produce Janus colloidal particles in large quantity." *Langmuir* **2006**, *22*, 9495-9499.

[19]   Kim, J. W.; Larsen, R. J.; Weitz, D. A. "Synthesis of nonspherical colloidal particles with anisotropic properties." *Journal of the American Chemical Society* **2006**, *128*, 14374-14377.

[20]   Nie, Z. H.; Li, W.; Seo, M.; Xu, S. Q.; Kumacheva, E. "Janus and ternary particles generated by microfluidic synthesis: Design, synthesis, and self-assembly." *Journal of the American Chemical Society* **2006**, *128*, 9408-9412.

[21]   Chen, C.-H.; Abate, A. R.; Lee, D.; Terentjev, E. M.; Weitz, D. A. "Microfluidic assembly of magnetic hydrogel particles with uniformly anisotropic structure." *Advanced Materials* **2009**, *21*, 3201-3204.

[22]   Shang, L.; Shangguan, F.; Cheng, Y.; Lu, J.; Xie, Z.; Zhao, Y.; Gu, Z. "Microfluidic generation of magnetoresponsive Janus photonic crystal particles." *Nanoscale* **2013**, *5*, 9553-7.

[23]   Nisisako, T.; Torii, T.; Takahashi, T.; Takizawa, Y. "Synthesis of monodisperse bicolored Janus particles with electrical anisotropy using a microfluidic co-flow system." *Advanced Materials* **2006**, *18*, 1152-+.

[24]   Williams, P. "Quorum sensing, communication and cross-kingdom signalling in the bacterial world." *Microbiology* **2007**, *153*, 3923-3938.

[25] Baroud, C. N.; Gallaire, F.; Dangla, R. "Dynamics of microfluidic droplets." *Lab Chip* **2010**, *10*, 2032-45.

[26] Garstecki, P.; Fuerstman, M. J.; Stone, H. A.; Whitesides, G. M. "Formation of droplets and bubbles in a microfluidic T-junction-scaling and mechanism of break-up." *Lab on a Chip* **2006**, *6*, 437-46.

[27] Zheng, B.; Tice, J. D.; Ismagilov, R. F. "Formation of droplets of in microfluidic channels alternating composition and applications to indexing of concentrations in droplet-based assays." *Analytical Chemistry* **2004**, *76*, 4977-4982.

[28] Hung, L. H.; Choi, K. M.; Tseng, W. Y.; Tan, Y. C.; Shea, K. J.; Lee, A. P. "Alternating droplet generation and controlled dynamic droplet fusion in microfluidic device for CdS nanoparticle synthesis." *Lab on a Chip* **2006**, *6*, 174-8.

[29] Jin, B. J.; Kim, Y. W.; Lee, Y.; Yoo, J. Y. "Droplet merging in a straight microchannel using droplet size or viscosity difference." *Journal of Micromechanics and Microengineering* **2010**, *20*, 035003.

[30] Kunqiang, J. Microfluidic Production of Polymeric Functional Microparticles, University of Maryland, College Park, 2012.

[31] Hu, J.; Zhou, S.; Sun, Y.; Fang, X.; Wu, L. "Fabrication, properties and applications of Janus particles." *Chemical Society Reviews* **2012**, *41*, 4356-4378.

[32] Casagrande, C.; Fabre, P.; Raphaël, E.; Veyssié, M. ""Janus Beads": Realization and Behaviour at Water/Oil Interfaces." *Europhysics Letters* **1989**, *9*, 251.

[33] Shum, H. C.; Lee, D.; Yoon, I.; Kodger, T.; Weitz, D. A. "Double Emulsion Templated Monodisperse Phospholipid Vesicles." *Langmuir* **2008**, *24*, 7651-7653.

[34] Chen, C. H.; Shah, R. K.; Abate, A. R.; Weitz, D. A. "Janus particles templated from double emulsion droplets generated using microfluidics." *Langmuir* **2009**, *25*, 4320-3.

[35] Dendukuri, D.; Pregibon, D. C.; Collins, J.; Hatton, T. A.; Doyle, P. S. "Continuous-flow lithography for high-throughput microparticle synthesis." *Nature Materials* **2006**, *5*, 365-369.

[36] Shum, H. C.; Abate, A. R.; Lee, D.; Studart, A. R.; Wang, B.; Chen, C. H.; Thiele, J.; Shah, R. K.; Krummel, A.; Weitz, D. A. "Droplet microfluidics for fabrication of non-spherical particles." *Macromolecular Rapid Communications* **2010**, *31*, 108-18.

[37] Shum, H. C.; Kim, J.-W.; Weitz, D. A. "Microfluidic Fabrication of Monodisperse Biocompatible and Biodegradable Polymersomes with Controlled Permeability." *Journal of the American Chemical Society* **2008**, *130*, 9543-9549.

[38] Ismagilov, R. F.; Schwartz, A.; Bowden, N.; Whitesides, G. M. "Autonomous movement and self-assembly." *Angewandte Chemie-International Edition* **2002**, *41*, 652-+.

[39] Gao, W.; Uygun, A.; Wang, J. "Hydrogen-Bubble-Propelled Zinc-Based Microrockets in Strongly Acidic Media." *Journal of the American Chemical Society* **2012**, *134*, 897-900.

[40] Solovev, A. A.; Sanchez, S.; Schmidt, O. G. "Collective behaviour of self-propelled catalytic micromotors." *Nanoscale* **2013**, *5*, 1284-93.

[41] Sattayasamitsathit, S.; Kou, H.; Gao, W.; Thavarajah, W.; Kaufmann, K.; Zhang, L.; Wang, J. "Fully Loaded Micromotors for Combinatorial Delivery and Autonomous Release of Cargoes." *Small* **2014**, *10*, 2830-2833.

[42] Gao, W.; D'Agostino, M.; Garcia-Gradilla, V.; Orozco, J.; Wang, J. "Multi-Fuel Driven Janus Micromotors." *Small* **2013**, *9*, 467-471.

[43] Fattah, Z.; Loget, G.; Lapeyre, V.; Garrigue, P.; Warakulwit, C.; Limtrakul, J.; Bouffier, L.; Kuhn, A. "Straightforward single-step generation of microswimmers by bipolar electrochemistry." *Electrochimica Acta* **2011**, *56*, 10562-10566.

[44] Baraban, L.; Tasinkevych, M.; Popescu, M. N.; Sanchez, S.; Dietrich, S.; Schmidt, O. G. "Transport of cargo by catalytic Janus micro-motors." *Soft Matter* **2012**, *8*, 48-52.

[45] Wang, Y.; Hernandez, R. M.; Bartlett, D. J.; Bingham, J. M.; Kline, T. R.; Sen, A.; Mallouk, T. E. "Bipolar electrochemical mechanism for the propulsion of catalytic nanomotors in hydrogen peroxide solutions." *Langmuir* **2006**, *22*, 10451-10456.

[46] Wilson, D. A.; Nolte, R. J. M.; van Hest, J. C. M. "Autonomous movement of platinum-loaded stomatocytes." *Nature Chemistry* **2012**, *4*, 268-274.

[47] Catchmark, J. M.; Subramanian, S.; Sen, A. "Directed rotational motion of microscale objects using interfacial tension gradients continually generated via catalytic reactions." *Small* **2005**, *1*, 202-206.

[48] Balasubramanian, S.; Kagan, D.; Hu, C. M. J.; Campuzano, S.; Lobo-Castanon, M. J.; Lim, N.; Kang, D. Y.; Zimmerman, M.; Zhang, L. F.; Wang, J. "Micromachine-Enabled Capture and Isolation of Cancer Cells in Complex Media." *Angewandte Chemie-International Edition* **2011**, *50*, 4161-4164.

[49] Gao, W.; Wang, J. "The Environmental Impact of Micro/Nanomachines. A Review." *Acs Nano* **2014**, *8*, 3170-3180.

[50] Guix, M.; Orozco, J.; Garcia, M.; Gao, W.; Sattayasamitsathit, S.; Merkoci, A.; Escarpa, A.; Wang, J. "Superhydrophobic Alkanethiol-Coated Microsubmarines for Effective Removal of Oil." *Acs Nano* **2012**, *6*, 4445-4451.

[51] Kline, T. R.; Paxton, W. F.; Mallouk, T. E.; Sen, A. "Catalytic nanomotors: remote-controlled autonomous movement of striped metallic nanorods." *Angew Chem Int Ed Engl* **2005**, *44*, 744-6.

[52] Subramanian, A.; Lin, H. Y. "Crosslinked chitosan: its physical properties and the effects of matrix stiffness on chondrocyte cell morphology and proliferation." *Journal of biomedical materials research. Part A* **2005**, *75*, 742-53.

[53] Javvaji, V. New Concepts for Genlation of Alginate and its Derivatives. PhD dissertation, University of Maryland 2013.

[54] Meijering, E. Imaging and Spectroscopic Analysis of Living Cells; Elsevier, 2012; Vol. 504 of Methods in Enzymology; pp 183-200.

[55] Pereira, C. S.; Thompson, J. A.; Xavier, K. B. *AI-2-mediated signalling in bacteria*, 2013; Vol. 37.

[56] Diaz, Z.; Xavier, K. B.; Miller, S. T. "The Crystal Structure of the Escherichia coli Autoinducer-2 Processing Protein LsrF." *PLoS ONE* **2009**, *4*, e6820.

[57] Tsao, C. Y.; Hooshangi, S.; Wu, H. C.; Valdes, J. J.; Bentley, W. E. "Autonomous induction of recombinant proteins by minimally rewiring native quorum sensing regulon of E. coli." *Metabolic Engineering* **2010**, *12*, 291-297.

[58] Thompson, Jessica A.; Oliveira, Rita A.; Djukovic, A.; Ubeda, C.; Xavier, Karina B. "Manipulation of the Quorum Sensing Signal AI-2 Affects the Antibiotic-Treated Gut Microbiota." *Cell Reports*, *10*, 1861-1871.

[59] Velegol, D.; Jerri, H. A.; McDermott, J. J.; Chaturvedi, N. "Microfactories for colloidal assemblies." *AIChE Journal* **2010**, *56*, 564-569.

[60] Jiang, K.; Xue, C.; Arya, C.; Shao, C.; George, E. O.; Devoe, D. L.; Raghavan, S. R. "A new approach to in-situ "micromanufacturing": Microfluidic fabrication of magnetic and fluorescent chains using chitosan microparticles as building blocks." *Small* **2011**.

[61] Sacanna, S.; Pine, D. J. "Shape-anisotropic colloids: Building blocks for complex assemblies." *Current Opinion in Colloid & Interface Science* **2011**, *16*, 96-105.

[62]   Shepherd, R. F.; Conrad, J. C.; Rhodes, S. K.; Link, D. R.; Marquez, M.; Weitz, D. A.; Lewis, J. A. "Microfluidic assembly of homogeneous and Janus colloid-filled hydrogel granules." *Langmuir* **2006**, *22*, 8618-8622.

[63]   Yuet, K. P.; Hwang, D. K.; Haghgooie, R.; Doyle, P. S. "Multifunctional superparamagnetic Janus particles." *Langmuir* **2010**, *26*, 4281-4287.

[64]   Prasad, N.; Perumal, J.; Choi, C.-H.; Lee, C.-S.; Kim, D.-P. "Generation of monodisperse inorganic-organic Janus microspheres in a microfluidic device." *Advanced Functional Materials* **2009**, *19*, 1656-1662.

[65]   Wu, H. C.; Tsao, C. Y.; Quan, D. N.; Cheng, Y.; Servinsky, M. D.; Carter, K. K.; Jee, K. J.; Terrell, J. L.; Zargar, A.; Rubloff, G. W.; Payne, G. F.; Valdes, J. J.; Bentley, W. E. "Autonomous bacterial localization and gene expression based on nearby cell receptor density." *Molecular Systems Biology* **2013**, *9*.

[66]   Xie, H.; She, Z. G.; Wang, S.; Sharma, G.; Smith, J. W. "One-Step Fabrication of Polymeric Janus Nanoparticles for Drug Delivery." *Langmuir* **2012**, *28*, 4459-4463.

[67]   Faria, J.; Ruiz, M. P.; Resasco, D. E. "Phase-Selective Catalysis in Emulsions Stabilized by Janus Silica-Nanoparticles." *Advanced Synthesis & Catalysis* **2010**, *352*, 2359-2364.

[68]   Chokkalingam, V.; Weidenhof, B.; Kramer, M.; Maier, W. F.; Herminghaus, S.; Seemann, R. "Optimized droplet-based microfluidics scheme for sol-gel reactions." *Lab on a Chip* **2010**, *10*, 1700-5.

[69]   Bremond, N.; Thiam, A.; Bibette, J. "Decompressing emulsion droplets favors coalescence." *Physical Review Letters* **2008**, *100*.

[70]   Niu, X.; Gulati, S.; Edel, J. B.; deMello, A. J. "Pillar-induced droplet merging in microfluidic circuits." *Lab on a Chip* **2008**, *8*, 1837-1841.

[71]   Deen, W. M. *Analysis of Transport Phenomena*; Oxford University Press, Inc: New York, 1998.

[72]   Wang, K.; Lu, Y.; Yang, L.; Luo, G. "Microdroplet coalescences at microchannel junctions with different collision angles." *AIChE Journal* **2013**, *59*, 643-649.

[73]   Mazutis, L.; Griffiths, A. D. "Selective droplet coalescence using microfluidic systems." *Lab on a Chip* **2012**, *12*, 1800-6.

[74] Christopher, G. F.; Bergstein, J.; End, N. B.; Poon, M.; Nguyen, C.; Anna, S. L. "Coalescence and splitting of confined droplets at microfluidic junctions." *Lab on a Chip* **2009**, *9*, 1102-9.

[75] Orozco, J.; Campuzano, S.; Kagan, D.; Zhou, M.; Gao, W.; Wang, J. "Dynamic Isolation and Unloading of Target Proteins by Aptamer-Modified Microtransporters." *Analytical Chemistry* **2011**, *83*, 7962-7969.

[76] Burdick, J.; Laocharoensuk, R.; Wheat, P. M.; Posner, J. D.; Wang, J. "Synthetic nanomotors in microchannel networks: Directional microchip motion and controlled manipulation of cargo." *Journal of the American Chemical Society* **2008**, *130*, 8164-+.

[77] Mori, K.; Yoshioka, N.; Kondo, Y.; Takeuchi, T.; Yamashita, H. "Catalytically active, magnetically separable, and water-soluble FePt nanoparticles modified with cyclodextrin for aqueous hydrogenation reactions." *Green Chemistry* **2009**, *11*, 1337.

[78] Rasband, W. S. ImageJ. **1997-2014**.

[79] Dyab, A. K. F.; Ozmen, M.; Ersoz, M.; Paunov, V. N. "Fabrication of novel anisotropic magnetic microparticles." *Journal of Materials Chemistry* **2009**, *19*, 3475.

[80] Hosta-Rigau, L.; Chung, S. F.; Postma, A.; Chandrawati, R.; Stadler, B.; Caruso, F. "Capsosomes with "Free-Floating" Liposomal Subcompartments." *Advanced Materials* **2011**, *23*, 4082-+.

[81] Hosta-Rigau, L.; Shimoni, O.; Stadler, B.; Caruso, F. "Advanced Subcompartmentalized Microreactors: Polymer Hydrogel Carriers Encapsulating Polymer Capsules and Liposomes." *Small* **2013**, *9*, 3573-3583.

[82] Siti, W.; de Hoog, H. P. M.; Fischer, O.; Shan, W. Y.; Tomczak, N.; Nallani, M.; Liedberg, B. "An intercompartmental enzymatic cascade reaction in channel-equipped polymersome-in-polymersome architectures." *Journal of Materials Chemistry B* **2014**, *2*, 2733-2737.

[83] van Dongen, S. F. M.; Nallani, M.; Cornelissen, J. L. L. M.; Nolte, R. J. M.; van Hest, J. C. M. "A Three-Enzyme Cascade Reaction through Positional Assembly of Enzymes in a Polymersome Nanoreactor." *Chemistry-a European Journal* **2009**, *15*, 1107-1114.

[84] De Geest, B. G.; De Koker, S.; Immesoete, K.; Demeester, J.; De Smedt, S. C.; Hennink, W. E. "Self-Exploding Beads Releasing Microcarriers." *Advanced Materials* **2008**, *20*, 3687-+.

[85]   Pekarek, K. J.; Jacob, J. S.; Mathiowitz, E. "Double-Walled Polymer Microspheres for Controlled Drug-Release." *Nature* **1994**, *367*, 258-260.

[86]   Chang, T. M. S. "Therapeutic applications of polymeric artificial cells." *Nature Reviews Drug Discovery* **2005**, *4*, 221-235.

[87]   Chang, T. M. S.; MacIntosh, F. C.; Mason, S. G. "SEMIPERMEABLE AQUEOUS MICROCAPSULES: I. PREPARATION AND PROPERTIES." *Canadian Journal of Physiology and Pharmacology* **1966**, *44*, 115-128.

[88]   Choi, C.-H.; Kang, S.-M.; Jin, S. H.; Yi, H.; Lee, C.-S. "Controlled Fabrication of Multicompartmental Polymeric Microparticles by Sequential Micromolding via Surface-Tension-Induced Droplet Formation." *Langmuir* **2014**, *31*, 1328-1335.

[89]   Wong, H.; Chang, T. M. S. "A NOVEL 2 STEP PROCEDURE FOR IMMOBILIZING LIVING CELLS IN MICROCAPSULES FOR IMPROVING XENOGRAFT SURVIVAL." *Biomaterials Artificial Cells and Immobilization Biotechnology* **1991**, *19*, 687-697.

[90]   Zhang, Y.; Ho, Y.-P.; Chiu, Y.-L.; Chan, H. F.; Chlebina, B.; Schuhmann, T.; You, L.; Leong, K. W. "A programmable microenvironment for cellular studies via microfluidics-generated double emulsions." *Biomaterials* **2013**, *34*, 4564-4572.

[91]   Stadler, B.; Price, A. D.; Chandrawati, R.; Hosta-Rigau, L.; Zelikin, A. N.; Caruso, F. "Polymer hydrogel capsules: en route toward synthetic cellular systems." *Nanoscale* **2009**, *1*, 68-73.

[92]   Dowling, M. B.; Bagal, A. S.; Raghavan, S. R. "Self-Destructing "Mothership" Capsules for Timed Release of Encapsulated Contents." *Langmuir* **2013**, *29*, 7993-7998.

[93]   Gupta, A.; Terrell, J. L.; Fernandes, R.; Dowling, M. B.; Payne, G. F.; Raghavan, S. R.; Bentley, W. E. "Encapsulated fusion protein confers "sense and respond" activity to chitosan-alginate capsules to manipulate bacterial quorum sensing." *Biotechnology and Bioengineering* **2013**, *110*, 552-562.

[94]   Krasaekoopt, W.; Bhandari, B.; Deeth, H. "The influence of coating materials on some properties of alginate beads and survivability of microencapsulated probiotic bacteria." *International Dairy Journal* **2004**, *14*, 737-743.

[95]   Zhou, Y.; Martins, E.; Groboillot, A.; Champagne, C. P.; Neufeld, P. C. "Spectrophotometric quantification of lactic bacteria in alginate and control of cell release with chitosan coating." *Journal of Applied Microbiology* **1998**, *84*, 342-348.

[96]   Chang, T. M. S. "Removal of endogenous and exogenous toxins by a microencapsulated absorbent." *Canadian Journal of Physiology and Pharmacology* **1969**, *47*, 1043-1045.

[97]   Weitz, M.; Muckl, A.; Kapsner, K.; Berg, R.; Meyer, A.; Simmel, F. C. "Communication and Computation by Bacteria Compartmentalized within Microemulsion Droplets." *Journal of the American Chemical Society* **2014**, *136*, 72-75.

[98]   Hol, F. J. H.; Dekker, C. "Zooming in to see the bigger picture: Microfluidic and nanofabrication tools to study bacteria." *Science* **2014**, *346*.

[99]   Kim, B. J.; Wu, M. "Microfluidics for Mammalian Cell Chemotaxis." *Annals of biomedical engineering* **2012**, *40*, 1316-1327.

[100]   Gupta, K.; Kim, D.-H.; Ellison, D.; Smith, C.; Kundu, A.; Tuan, J.; Suh, K.-Y.; Levchenko, A. "Lab-on-a-chip devices as an emerging platform for stem cell biology." *Lab on a Chip* **2010**, *10*, 2019-2031.

[101]   Cheng, Y.; Tsao, C. Y.; Wu, H. C.; Luo, X. L.; Terrell, J. L.; Betz, J.; Payne, G. F.; Bentley, W. E.; Rubloff, G. W. "Electroaddressing Functionalized Polysaccharides as Model Biofilms for Interrogating Cell Signaling." *Advanced Functional Materials* **2012**, *22*, 519-528.

[102]   Boedicker, J. Q.; Vincent, M. E.; Ismagilov, R. F. "Microfluidic Confinement of Single Cells of Bacteria in Small Volumes Initiates High-Density Behavior of Quorum Sensing and Growth and Reveals Its Variability." *Angewandte Chemie (International ed. in English)* **2009**, *48*, 5908-5911.

[103]   Kim, B. J.; Park, T.; Moon, H. C.; Park, S.-Y.; Hong, D.; Ko, E. H.; Kim, J. Y.; Hong, J. W.; Han, S. W.; Kim, Y.-G.; Choi, I. S. "Cytoprotective Alginate/Polydopamine Core/Shell Microcapsules in Microbial Encapsulation." *Angewandte Chemie* **2014**, *126*, 14671-14674.

[104]   Liouni, M.; Drichoutis, P.; Nerantzis, E. "Studies of the mechanical properties and the fermentation behavior of double layer alginate–chitosan beads, using Saccharomyces cerevisiae entrapped cells." *World Journal of Microbiology and Biotechnology* **2008**, *24*, 281-288.